

**NIST-GCR-97-721**

---

---

**MIXING AND RADIATION PROPERTIES OF  
BUOYANT LUMINOUS FLAME  
ENVIRONMENTS**

---

---

Z. Dai, S.S. Krishnan, K.-C. Lin, R. Sangras,  
J.S. Wu, and G.M. Faeth

**NIST**

United States Department of Commerce  
Technology Administration  
National Institute of Standards and Technology

NIST-GCR-97-721

---

---

# MIXING AND RADIATION PROPERTIES OF BUOYANT LUMINOUS FLAME ENVIRONMENTS

---

---

Z. Dai, S.S. Krishnan, K.-C. Lin, R. Sangras,  
J.S. Wu, and G.M. Faeth  
Department of Aerospace Engineering  
The University of Michigan  
Ann Arbor, Michigan 48109-2118

October, 1996  
Building and Fire Research Laboratory  
National Institute of Standards and Technology  
Gaithersburg, MD 20899-0001

Issued August, 1997



U.S. Department of Commerce  
William M. Daley, *Secretary*  
Technology Administration  
Mary L. Good, *Under Secretary for Technology*  
National Institute of Standards and Technology  
Robert E. Hebner, *Acting Director*

### Notice

This report was prepared for the Building and Fire Research Laboratory of the National Institute of Standards and Technology under grant number 60NANB4D1696. The statement and conclusions contained in this report are those of the authors and do not necessarily reflect the views of the National Institute of Standards and Technology or the Building and Fire Research Laboratory.

**MIXING AND RADIATION PROPERTIES OF BUOYANT  
LUMINOUS FLAME ENVIRONMENTS**

October 1996

Sponsored by:

U.S. Department of Commerce  
National Institute of Standards and Technology  
(formerly National Bureau of Standards)  
Laboratory for Building and Fire Research  
Washington, D.C. 20234

## Abstract

An investigation of the radiation and mixing properties of buoyant turbulent diffusion flames is described. The study was divided into two phases: (1) the consideration of the optical and radiative properties of soot, which must be understood in order to develop nonintrusive methods for measuring soot properties and to estimate the continuum radiation properties of soot in flame environments, and (2) the consideration of the structure and mixing properties of buoyant turbulent plumes, which must be understood in order to resolve effects of turbulence/radiation interactions and to benchmark computationally tractable models of buoyant turbulent flows. Consideration of the optical and radiative properties of soot involved evaluation of the Rayleigh-Debye-Gans (RDG) scattering approximation for soot aggregates and the use of this theory to measure the refractive index properties and dimensionless extinction coefficients in the visible (350-800 nm) of soot emitted from buoyant turbulent diffusion flames in the long residence time regime where emitted soot properties are independent of position in the flame and flame residence time. Soot from both gas- and liquid hydrocarbon-fueled flames was considered, including acetylene, propylene, ethylene, propane, toluene, benzene, cyclohexane and n-heptane fueled flames burning in air. Measured soot optical properties were in reasonably good agreement with RDG predictions, even though optical size parameters for individual primary soot particles reached values as large as 0.46 over the test range, which are the largest values of this parameter considered thus far. It was also found that soot fractal dimensions were independent of fuel type and had an average value of 1.78 with a standard deviation of 0.02, which is in good agreement with the earlier measurements of Köylü and Faeth (1994a) for similar soot. Soot refractive index properties did not vary significantly with fuel type, compared with experimental uncertainties, in spite of significant variations of soot composition and morphological properties over the test range. Present soot refractive index properties also are in reasonably good agreement with the often criticized measurements of Dalzell and Sarofim (1969). Furthermore, soot refractive index properties did not exhibit a resonance condition in the near uv, supporting similar observations of Vaglieco et al. (1990). Finally, present dimensionless extinction coefficients were relatively independent of fuel type and wavelength over the test range yielding a mean value of 5.7 with a standard deviation of 0.7; this value is in good agreement with earlier measurements of Wu et al. (1997) in this laboratory but is significantly lower than values in the range 8.1-9.4 reported by Dobbins et al. (1994) and Choi et al. (1995) for reasons that still must be explained.

Study of the structure and mixing properties of buoyant turbulent plumes involved consideration of free turbulent line plumes, emphasizing self-preserving conditions where effects of source disturbances have been lost. It was found that self-preserving behavior was observed for heights above the source exceeding 75 source widths and 10 Morton length scales and yielded flows that were up to 60% narrower with scaled values at the axis up to 20% different from earlier results in the literature that were obtained nearer to the source (less than 60 source widths). Cross-stream distributions of mixture fraction fluctuations did not exhibit a dip near the axis and had a fluctuation intensity of roughly 48%, which is similar to results for self-preserving round turbulent plumes; this behavior suggests strong effects of buoyancy/turbulence interactions in these flows. Finally, self-preserving free plane turbulent plumes mix much more rapidly than corresponding turbulent adiabatic wall plumes because the presence of the wall inhibits large eddy motion within the wall plumes. Finally, present observations of plane turbulent wall plumes have been drawn from extensive development tests of the experimental apparatus and should be considered to be preliminary pending final measurements that are currently in progress.

### Acknowledgments

This research was supported by the United States Department of Commerce, National Institute of Standards and Technology (formerly National Bureau of Standards), Grant No. 60NANB4D1696, with H.R. Baum of the Laboratory for Building and Fire Research serving as Scientific Officer.

## Table of Contents

Abstract .....	iv
Acknowledgments.....	v
List of Tables.....	vii
List of Figures .....	viii
Nomenclature:Soot Optical Properties .....	x
Nomenclature:Buoyant Turbulent Plumes.....	xiii
1. Introduction.....	1
2. Optical and Radiative Properties of Soot.....	2
2.1 Introduction .....	2
2.2 Experimental Methods .....	6
2.3 Theoretical Methods.....	13
2.4 Results and Discussion.....	15
2.5 Conclusions.....	26
3. Buoyant Turbulent Plumes .....	31
3.1 Introduction .....	31
3.2 Experimental Methods .....	40
3.3 Results and Discussion.....	43
3.4 Conclusions.....	50
References .....	50

## List of Tables

<u>Table</u>	<u>Titles</u>	<u>Page</u>
1.	Light sources used for measurements of scattering from soot.....	12
2.	Summary of test conditions for round buoyant turbulent diffusion flames in the long residual time regime .....	16
3.	Summary of the depolarization ratios: hydrocarbon-fueled flames .....	20
4.	Soot optical properties: gas-fueled flames .....	27
5.	Soot optical properties: liquid-fueled flames.....	28
6.	Soot optical properties: hydrocarbon-fueled flames .....	29
7.	Scaling of self-preserving turbulent plumes .....	32
8.	Plane buoyant turbulent plume test conditions.....	44
9.	Summary of self-preserving plane turbulent plume constants.....	49

## List of Figures

<u>Figure</u>	<u>Caption</u>	<u>Page</u>
1.	Sketch of simulated soot particles as a mass fractal aggregates.....	3
2.	Sketch of the buoyant turbulent diffusion flame apparatus.....	7
3.	Sketch of the gas-fueled diffusion flame burner.....	8
4.	Sketch of the liquid-fueled diffusion flame burner.....	9
5.	Sketch of the radiation extinction and scattering instrument.....	11
6.	Measured and predicted angular scattering patterns at 514.5 nm for Rayleigh scattering of gaseous propane.....	14
7.	Measured and predicted angular scattering patterns at 351.2 nm for overfire soot aggregates in buoyant turbulent toluene/air diffusion flames.....	18
8.	Measured and predicted angular scattering patterns at 632.8 nm for overfire soot aggregates in buoyant turbulent propane/air diffusion flames.....	19
9.	Measured and predicted volumetric vv differential scattering cross-sections at 632.8 nm as functions of the modulus of the scattering vector for overfire soot aggregates in buoyant turbulent acetylene, propylene, ethylene and propane/air diffusion flames.....	21
10.	Measured refractive index functions, E(m) and F(m), in the visible (350-800 nm) for overfire soot aggregates in buoyant, turbulent diffusion flames.....	23
11.	Measured refractive indices of soot in the near ultraviolet and visible portions of the spectrum. Measurements of Batten (1985), Chang and Charalampopoulos (1990), Dalzell and Sarofim (1969), Wu et al. (1997) and the present study.....	24
12.	Measured dimensionless extinction coefficients in the visible portion of the spectrum. Measurements of Choi et al. (1995), Dobbins et al. (1994), Wu et al. (1997) and the present study.....	30
13.	Sketch of the round buoyant turbulent plume test apparatus.....	34
14.	Radial profiles of mean mixture fractions in round buoyant turbulent plumes. From Dai et al. (1994).....	35
15.	Radial profiles of r.m.s. mixture fraction fluctuations in round buoyant turbulent plumes. From Dai et al. (1994).....	36

<u>Figure</u>	<u>Caption</u>	<u>Page</u>
16.	Radial profiles of mean streamwise velocities in self-preserving round buoyant turbulent plumes. From Dai et al. (1995a) .....	37
17.	Radial profiles of r.m.s. velocity fluctuations in self-preserving round buoyant turbulent plumes. From Dai et al. (1995a) .....	39
18.	Sketch of the plane buoyant turbulent plume apparatus.....	41
19.	Cross-stream profiles of mean mixture fractions in plane buoyant turbulent plumes .....	46
20.	Cross-stream profiles of r.m.s. fluctuating mixture fractions in plane buoyant turbulent plumes .....	47

### Nomenclature: Soot Optical Properties

C	=	optical cross section
d	=	burner diameter
$d_p$	=	primary particle diameter
$D_f$	=	mass fractal dimension, Eq. (1)
$E(m)$	=	refractive index function = $\text{Im}((m^2-1)/(m^2+2))$
$f_v$	=	soot volume fraction
$g(\lambda, R_g, D_f)$	=	aggregate total scattering factor
$F(m)$	=	refractive index function = $ (m^2-1)/(m^2+2) ^2$
i	=	$(-1)^{1/2}$
I	=	light intensity
k	=	wave number = $2\pi/\lambda$
$k_e$	=	dimensionless extinction coefficient
$k_{eR}$	=	$k_e$ at the Rayleigh scattering limit, Eq. (8)
$k_f$	=	fractal prefactor, Eq. (1)
L	=	light path length, mean flame length
m	=	soot refractive index = $n+i\kappa$
n	=	real part of soot refractive index
$n_p$	=	mean number of primary particles per unit volume
N	=	number of primary particles per aggregate
q	=	modulus of scattering vector = $2k\sin(\theta/2)$
Q	=	volumetric optical cross section
Re	=	Reynolds number of burner = $u_0 d/v_0$

$R_g$	=	radius of gyration of an aggregate
$t_r$	=	characteristic flame residence time
$t_s$	=	characteristic flame residence time at laminar smoke point
$T_s$	=	gas temperature at measurement condition
$u$	=	streamwise gas velocity
$x_p$	=	primary particle size parameter= $\pi d_p/\lambda$
$\theta$	=	angle of scattering from forward direction
$\kappa$	=	imaginary part of refractive index of soot
$\lambda$	=	wavelength of radiation
$\nu$	=	kinematic viscosity
$\rho$	=	gas density
$\rho_s$	=	density of soot
$\rho_{sa}$	=	ratio of scattering to absorption cross sections
$\rho_v$	=	depolarization ratio, Eq. (10)

### Subscripts

$a$	=	absorption
$c$	=	centerline value
$d$	=	differential
$e$	=	extinction
$h$	=	horizontal polarization
$ij$	=	incident (i) and scattered (j) polarization directions
$s$	=	total scattering
$v$	=	vertical polarization

### Superscripts

$o$	=	burner or light source exit condition
-----	---	---------------------------------------

- a = aggregate property
- p = primary particle property
- ( $\bar{\quad}$ ) = mean value over a polydisperse aggregate population

## Nomenclature: Buoyant Turbulent Plumes

$b$	=	source width
$B_o$	=	source buoyancy flux
$d$	=	source diameter
$f$	=	mixture fraction
$F(r \text{ or } y/(x-x_o))$	=	scaled cross-stream distribution of $\bar{f}$ in self-preserving region
$Fr_o$	=	source Froude number
$g$	=	acceleration of gravity
$k_f$	=	plume width coefficients, based on $\bar{f}$ , Eqs. (11) and (12)
$\ell_f$	=	characteristic plume radii based on $\bar{f}$ , Eqs. (11) and (12)
$\ell_M$	=	Morton length scale
$M_o$	=	source specific momentum flux
$Q$	=	plume volume flux
$r$	=	radial distance
$Re_o$	=	source Reynolds number, $u_o d/v_o$ or $u_o b/v_o$
$u$	=	streamwise velocity
$U(r \text{ or } y/(x-x_o))$	=	scaled cross-stream distribution of $\bar{u}$ in self-preserving region
$x$	=	streamwise distance
$y$	=	cross-stream distance
$\nu$	=	kinematic viscosity
$\rho$	=	density

## Subscripts

$c$	=	centerline value
$o$	=	initial value or virtual origin location
$\infty$	=	ambient value

## **Superscripts**

$(\bar{\quad})$  = time-averaged mean value

$(\overline{\quad})'$  = root-mean-squared fluctuating value

## 1. Introduction

An investigation is described that is relevant to two aspects of unwanted fires: (1) effects of fuel type and flame condition on the optical and radiative properties of soot in flame environments, and (2) the structure and mixing properties of buoyant turbulent flows typical of fire environments. The findings of the research have applications to modeling unwanted fires; to controlling the emission of radiant energy, toxic materials and soot from fires; to developing materials test codes for fire properties; and to developing fire detectors.

The first phase of the research is addressing the optical and radiative properties of soot in flame environments. The motivation for this investigation is that earlier results demonstrated a strong correlation between carbon monoxide and soot emissions from turbulent diffusion flames (Köylü et al., 1991; Köylü and Faeth, 1991), while continuum radiation from soot is the main radiative effect in practical fires (Köylü and Faeth, 1993). Understanding the optical properties of soot is crucial for a better understanding of both of these problems: soot concentrations and structure generally are measured using nonintrusive laser-based methods that require knowledge about soot optical properties in order to correctly interpret the measurements, while soot optical properties are a controlling factor in the continuum radiation properties of flames. Past work showed that soot morphology could be approximated by mass fractal aggregates of spherical primary particles, where the primary particles were nearly monodisperse while the aggregates exhibited broad distributions of the number of primary particles per aggregate, in agreement with earlier work (Köylü and Faeth, 1992). Then the use of the Rayleigh-Debye-Gans (RDG) scattering approximation, while approximating soot aggregates as polydisperse mass fractal objects, was shown to be acceptable for soot within diffusion flames based on evaluation of the approximate RDG predictions by both measurements and more exact predictions (Köylü and Faeth, 1994a,b; Farias et al., 1995). Subsequently, soot structure properties needed for RDG predictions of soot optical properties were studied, considering relationships between actual and projected soot images, and the mass fractal dimensions and prefactors of soot in flames (Köylü et al., 1995). These results also showed that the main limitation preventing reliable nonintrusive measurements of soot properties in flames, as well as reliable estimates of the continuum radiation properties of soot in flames, was inadequate information about the refractive indices of soot. Thus, the objective of this phase of the investigation is to experimentally determine effects of fuel type and flame condition on soot refractive index properties, and closely-associated properties such as dimensionless extinction coefficients, for wavelengths ranging from the near ultra-violet to the infra-red (350-5000 nm) which covers the wavelength range relevant to practical soot optical property and radiation applications.

The second phase of the research is addressing the properties of buoyant turbulent flows that are a central feature of the environment of unwanted fires and are needed in order to understand turbulence/radiation interactions. In particular, stochastic simulation techniques have been developed to estimate effects of turbulence/radiation interactions in flames, based on laminar flamelet concepts and a knowledge of mixture fraction statistics, see Kounalakis et al. (1991) and references cited therein. In spite of extensive past studies, however, available information about the turbulence properties of buoyant turbulent flows was too limited to allow use of the stochastic simulation methodology to estimate effects of turbulence/radiation interactions. Furthermore, the first phase of the present investigation revealed that past work had not completed measurements sufficiently far from the source to observe fully-developed (self-preserving) buoyant turbulent plume behavior (Dai and Faeth, 1996; Dai et al., 1994a,b,1995a,b). This finding is problematical because self-preserving conditions are important for developing models of buoyant turbulent flows that are needed to address problems of practical fire environments. Thus, the objective of this phase of the investigation is to experimentally determine the mean and turbulent properties of self-preserving buoyant turbulent plumes, and to use these results to evaluate models of plume structure and turbulence properties.

The studies of soot optical properties and buoyant turbulent plumes are described, in turn, in the following. The present description is brief; therefore, other publications resulting from the investigation should be studied for more details, e.g., Dai and Faeth (1996), Dai et al. (1994a,b,1995a,b), Faeth (1997), Faeth and Köylü (1995, 1996), Farias et al. (1995), Köylü (1992), Köylü and Faeth (1992,1993,1994a,b,1996), Krishnan et al. (1997), Wu et al. (1997), and Köylü et al. (1991,1995). The description of each phase of the research is sufficiently complete, however, so that it can be read independently.

## 2. Optical and Radiative Properties of Soot

### 2.1 Introduction

Practical hydrocarbon-fueled flames contain and emit soot, which affects their radiation, structure, toxic substance emission and pollutant emission properties. These effects have motivated considerable interest in the structure and optical properties of soot, in order to develop nonintrusive methods for measuring soot properties and to estimate the continuum radiation properties of soot in flame environments. Motivated by these observations, this phase of the investigation seeks a better understanding of soot optical and radiation properties in flame environments. Earlier work on this phase of the investigation addressed the morphological properties of soot and the applicability of the Rayleigh-Debye-Gans (RDG) scattering approximation to treat the optical properties of soot over the visible and infra-red wavelength ranges; current work on this phase of the investigation is addressing the refractive index properties of soot.

Earlier work concerning the structure and optical properties of soot only will be discussed briefly, more details can be found in the reviews by Charalampopoulos (1992), Faeth (1997), Faeth and Köylü (1995,1996), Faeth et al. (1989,1990), Jullien and Botet (1987), Köylü and Faeth (1993), Tien and Lee (1982) and Viskanta and Mengüç (1987). In addition, earlier work in this laboratory dealing with these properties is described by Faeth and Köylü (1995), Faeth et al. (1989, 1990), Farias et al. (1995), Köylü and Faeth (1992,1993,1994a,b,1996), and Köylü et al. (1995). In the following, the structure and optical properties of soot will be discussed in turn.

Numerous earlier studies have shown that soot consists of small spherical primary particles, having nearly constant diameters at a particular flame condition, collected into open structured aggregates that have broad distributions of the number of primary particles (Dalzell et al., 1970; Dobbins and Megaridis, 1987,1991; Dobbins et al., 1994; Erickson et al., 1964; Jullien and Botet, 1987; Martin and Hurd, 1987; Megaridis and Dobbins, 1990; Samson et al., 1987; Wersborg et al., 1972). Typical examples of soot aggregate structure can be seen from the simulated images illustrated in Fig. 1. In particular, distributions of primary particle diameters have standard deviations of 15-25% of the mean primary particle diameter while soot aggregates exhibit log-normal size distribution functions with aggregate sizes in the range 30-1800 primary particles. It also is generally agreed that flame-generated soot aggregates exhibit mass fractal-like behavior with a Hausdorff or fractal dimension,  $D_f < 2$ , even when the number of primary particles in an aggregate is small, which implies (Jullien and Botet, 1987):

$$N = k_f(R_g/d_p)^{D_f} \quad (1)$$

Earlier work has established that the fractal properties of soot aggregates in flame environments are relatively durable, yielding current best estimates of  $D_f = 1.82$  with an uncertainty (95% confidence) of 0.08 and  $k_f = 8.5$  with an uncertainty (95% confidence) of 0.5 (Köylü et al., 1995).

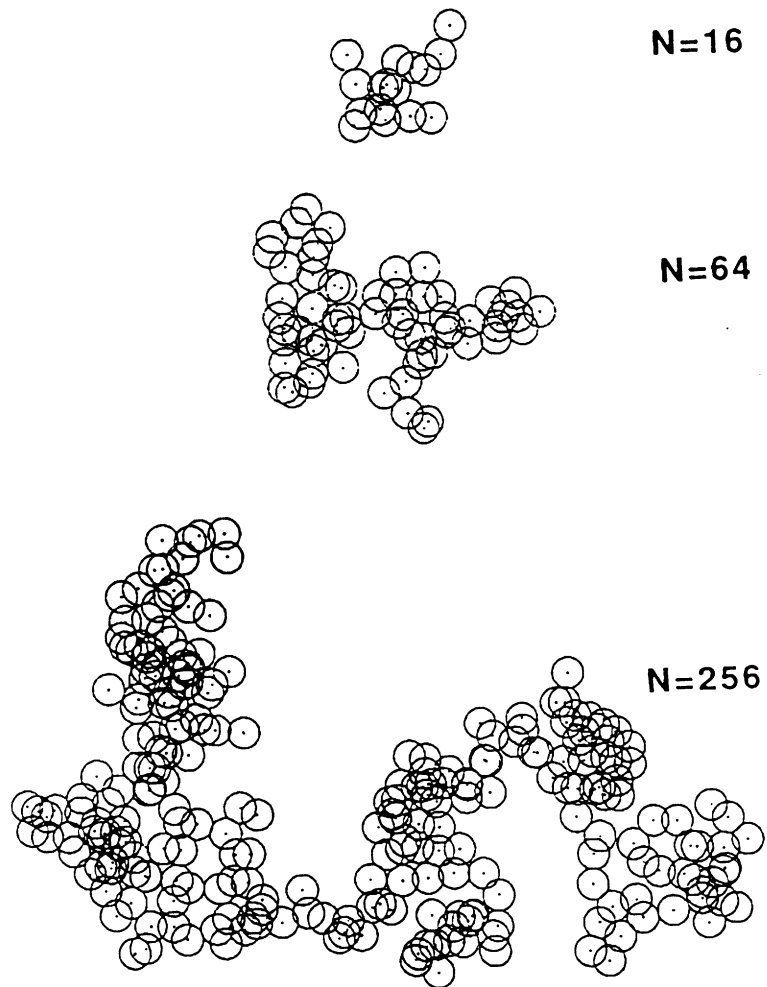


Fig. 1 Sketch of simulated soot particles as a mass fractal aggregates.

Measurements have shown that flame-generated soot ranges from small aggregates (dimensions on the order of 10 nm) near the start of soot formation, to large aggregates (dimensions on the order of 1  $\mu\text{m}$ ) emitted from large buoyant turbulent diffusion flames (Köylü and Faeth, 1992,1993,1994a,b). Thus, even though primary particle diameters are less than 60nm, which implies Rayleigh scattering from individual primary particles for wavelengths of practical interest, use of traditional approximate scattering theories has not been very effective (Köylü and Faeth, 1994a,b). These difficulties were established by direct measurements of soot scattering properties during early work (Erickson et al., 1964; Dalzell et al., 1970; Wersborg et al., 1972); for example, strong forward scattering was observed which is not representative of Rayleigh scattering behavior, while use of the Mie scattering approximation for an equivalent sphere still did not provide an adequate fit of the scattering measurements. The former behavior follows because the larger soot aggregates in the size distribution dominate scattering properties and are too large to be approximated as Rayleigh scattering objects (Köylü and Faeth, 1993); the latter behavior follows because  $D_p \ll \lambda$  which implies that aggregate structure is too open to be represented by a compact object such as an equivalent Mie scattering sphere (Berry and Percival, 1986). The limitations of the Rayleigh and Mie scattering theories prompted subsequent development of optical theories of soot aggregates based on the Rayleigh-Debye-Gans (RDG) approximation for mass fractal objects consisting of constant diameter spherical primary particles that just touch one another, and satisfy the Rayleigh scattering approximation as individual particles, with polydisperse aggregate size distributions (Jullien and Botet, 1987; Köylü and Faeth, 1993, 1994a,b; Martin and Hurd, 1987; Dobbins and Megaridis, 1991). The resulting RDG theory, which will be denoted RDG-PFA theory in the following, was questioned, however, because the relatively large refractive indices of soot raised concerns about the validity of the RDG scattering approximation (Köylü and Faeth, 1993).

In view of concerns about the RDG scattering approximation for soot aggregates, earlier work in this laboratory sought an experimental and computational evaluation of RDG-PFA theory (Köylü and Faeth, 1993,1994a,b; Farias et al., 1995). The experimental evaluation involved comparing RDG-PFA scattering predictions, based on measured soot structure properties from thermophoretic sampling and TEM analysis, with *in situ* measurements of scattering for the same aggregate population. This study considered both large soot aggregates in the fuel-lean (overfire) region of buoyant turbulent diffusion flames in the long residence time regime, where soot properties become independent of position in the overfire region and residence time, see Sivathanu and Faeth (1990) and Köylü and Faeth (1992), which emphasized the large-angle (power-law) regime (Köylü and Faeth (1994a), and small soot aggregates in the fuel-rich (underfire) region of laminar diffusion flames, which emphasized the small angle (Guinier) regime (Köylü and Faeth, 1994b). The predictions and measurements agreed within experimental uncertainties for the power-law regime, where soot aggregate properties that dominate aggregate scattering properties could be found accurately from structure measurements. The evaluation was less than definitive in the Guinier regime, however, due to difficulties of accurately measuring both scattering properties at small angles and the higher moments of the aggregate size distribution functions (e.g.,  $\bar{N}^2$ ) that dominate scattering properties at small angles (Köylü and Faeth, 1994a,b). This limitation of the experimental evaluation of RDG-PFA theory was a concern because multiple scattering effects that could compromise the use of RDG-PFA theory are most significant in the Guinier regime (Nelson, 1989a,b).

Farias et al. (1995) undertook a subsequent computational evaluation of RDG-PFA theory in order to obtain more definitive results in the Guinier regime. This evaluation was initially based on computations using the ICP formulation of Iskander et al. (1989) which provides a more exact treatment of the Guinier regime than RDG-PFA theory by including effects of multiple and self-induced scattering. Notably, Ku and Shim (1992) review several theories of aggregate optical properties that are more accurate than the RDG approximation, concluding that the ICP formulation was superior to the popular Jones and

Purcell-Pennypacker solutions. Subsequently, Lou and Charalampopoulos (1994) find improved results from the ICP approach using the Goedecke-O'Brian (GO) solution which provides a more exact treatment of the optical theorem (energy conservation); however, differences between ICP and GO predictions are negligible compared to computational uncertainties (roughly 10%) for conditions of present interest (Farias et al., 1995). In addition, problems of adequately defining the size distribution functions of polydisperse aggregates during experiments were avoided by using numerical simulations to generate aggregates having prescribed sizes and fractal properties. This computational evaluation was carried out for  $x_p \leq 0.4$  and  $N \leq 512$  for mass fractal objects having fractal and refractive index properties typical of soot (notably, this range of  $x_p$  also is typical of soot in the visible portion of the spectrum that is used for soot laser diagnostics). Evaluation of the ICP algorithm using Mie scattering predictions indicated satisfactory performance in the Guinier regime for conditions of interest, with progressive build-up of errors as  $x_p$ , the refractive index and the scattering angle increased into the power-law regime. Finally, the ICP and RDG-PFA predictions agreed within computational uncertainties, roughly 10%, within the Guinier regime. Thus, taken together, the combined experimental and computational evaluations suggest that the RDG-PFA theory is satisfactory for  $x_p \leq 0.4$  for refractive indices typical of soot, which covers the range of conditions normally encountered for flame-generated soot.

Given successful evaluation of the RDG-PFA theory for the optical properties of soot, there is potential for developing methods for solving the inverse problem so that soot structure properties can be found nonintrusively from scattering measurements and for treating continuum radiation from soot in flame environments. Unfortunately, this potential has not been realized due to large uncertainties concerning soot refractive indices in the critical visible and infrared wavelength regimes (Chang and Charalampopoulos, 1990; Choi et al., 1994, 1995; Dobbins et al., 1997; Köylü and Faeth, 1993; Sorensen et al., 1992a,b). Conventional wisdom is that soot refractive indices are relatively independent of fuel type, temperature and residence time in the flame. Nevertheless, some recent work finds variations of soot refractive indices with residence time in flame environments, and potentially large effects of fuel type, see Chang and Charalampopoulos (1990) and references cited therein. Thus, in spite of recent measurements by Choi et al. (1994, 1995), Köylü and Faeth (1994a) and Dobbins et al. (1997), which tend to support the classical soot refractive index measurements of Dalzell and Sarofim (1969), widespread criticism of these measurements has not yet been resolved (Tien and Lee, 1982). These difficulties are a substantial impediment to progress toward developing methods for predicting the continuum radiation properties of flames; in fact, potential errors caused by uncertainties concerning soot refractive indices are far larger than differences between the Rayleigh and RDG-PFA scattering theories for typical soot aggregates (Köylü and Faeth 1994a,b).

In view of these considerations, this phase of the investigation seeks to advance our understanding of soot refractive indices in flame environments by completing an experimental study of the effects of fuel type and flame conditions on soot refractive indices in the visible and infrared wavelength ranges. This work has involved *in-situ* measurements of soot scattering properties which are subsequently interpreted using RDG-PFA theory to find soot refractive indices and other soot optical properties. Thus far, measurements have been limited to soot in the overfire region of large gas- and liquid-fueled buoyant turbulent diffusion flames in the long residence time regime, where soot properties became universal for a particular fuel type burning in air (Köylü and Faeth, 1992).

The discussion begins with consideration of experimental and theoretical methods. Results are then presented, considering soot scattering properties, refractive index properties and dimensionless extinction coefficients, in turn.

## 2.2 Experimental Methods

Apparatus. A sketch of the test apparatus appears in Fig. 2. The arrangement is similar to earlier work considering overfire soot in the long residence time regime of buoyant turbulent diffusion flames (Köylü and Faeth, 1992,1994a). The components of the apparatus include a burner, a soot collection system and an exhaust system. The burner and soot collection system were located within a large outer enclosure (2400 x 2400 x 3600 mm high). The enclosure had a metal hood at the top and an adjustable exhaust system to collect and remove combustion products. The side walls of the enclosure are plastic strips which minimize effects of room disturbances.

The experimental program involved combustion of gaseous- and liquid-hydrocarbon fuels as buoyant turbulent diffusion flames in the long residence time regime where past work of Köylü and Faeth (1991,1992) and Sivathanu and Faeth (1990) has shown that soot properties in the overfire region are independent of position in the overfire region and flame residence time. A sketch of the gas-fueled burner is illustrated in Fig. 3. This burner follows the design of Sivathanu and Faeth (1990). The burner had a 50 mm diameter with a bed of metal beads used to disperse the fuel gas. The rim of the burner is water-cooled to prevent premature decomposition of the fuel. The fuels were injected vertically upward from the burner with the flames stabilizing naturally at the burner exit, yielding strongly buoyant, pool-like turbulent flames. Fuels considered included acetylene, propylene, ethylene and propane with fuel flow rates monitored using a rotameter.

Fuels considered included toluene, benzene, cyclohexane and n-heptane with fuel flow rates controlled using a positive-displacement liquid pump (Sci. Log ACCU Pump model FM-40) and monitored using a rotameter. A sketch of a typical liquid-fueled burner appears in Fig. 4. These burners involve a vertical cylindrical section. The bottom of the cylindrical burner was filled with round beads both to block radiative heat transfer for the base of the burner and to reduce the inventory of liquid fuel in the burner system. Vaporization of the liquid fuels themselves seemed to maintain burner temperatures to reasonable levels. These flames burned as naturally-attached turbulent pool fires above the burner port.

Soot properties were measured by collecting the combustion products in a sampling hood and duct that were heated to prevent thermophoretic deposition of soot on their surfaces. The exhaust duct had a diameter of 152 mm, with the measuring station at the exit of the duct. This duct discharged into the main hood of the apparatus. Note that since the soot structure, and the generation of soot per kg of fuel carbon burned, are independent of position in the overfire region for operation within the long residence time regime and (Sivathanu and Faeth, 1990; Köylü and Faeth, 1992), collection in this manner does not affect soot structure properties. Properties across the exit of the heated duct were generally uniform; nevertheless, soot concentrations did vary slightly based on gravimetric measurements of soot volume functions; therefore, this variation was considered when evaluating measurements of extinction which involved soot concentrations across the exit of the duct. Other soot property variations across the duct exit were ignored, however, which is consistent with overfire soot properties in the long residence time regime of buoyant turbulent diffusion flames.

Instrumentation. Several measurements are made in order to determine soot scattering properties, soot refractive index properties and the dimensionless extinction coefficients of soot, including: soot structure, soot density, temperature distributions along the optical path, a gravimetric determination of soot volume fraction and finally, extinction and scattering measurements at the wavelengths of interest. These measurements will be discussed, in turn, in the following.

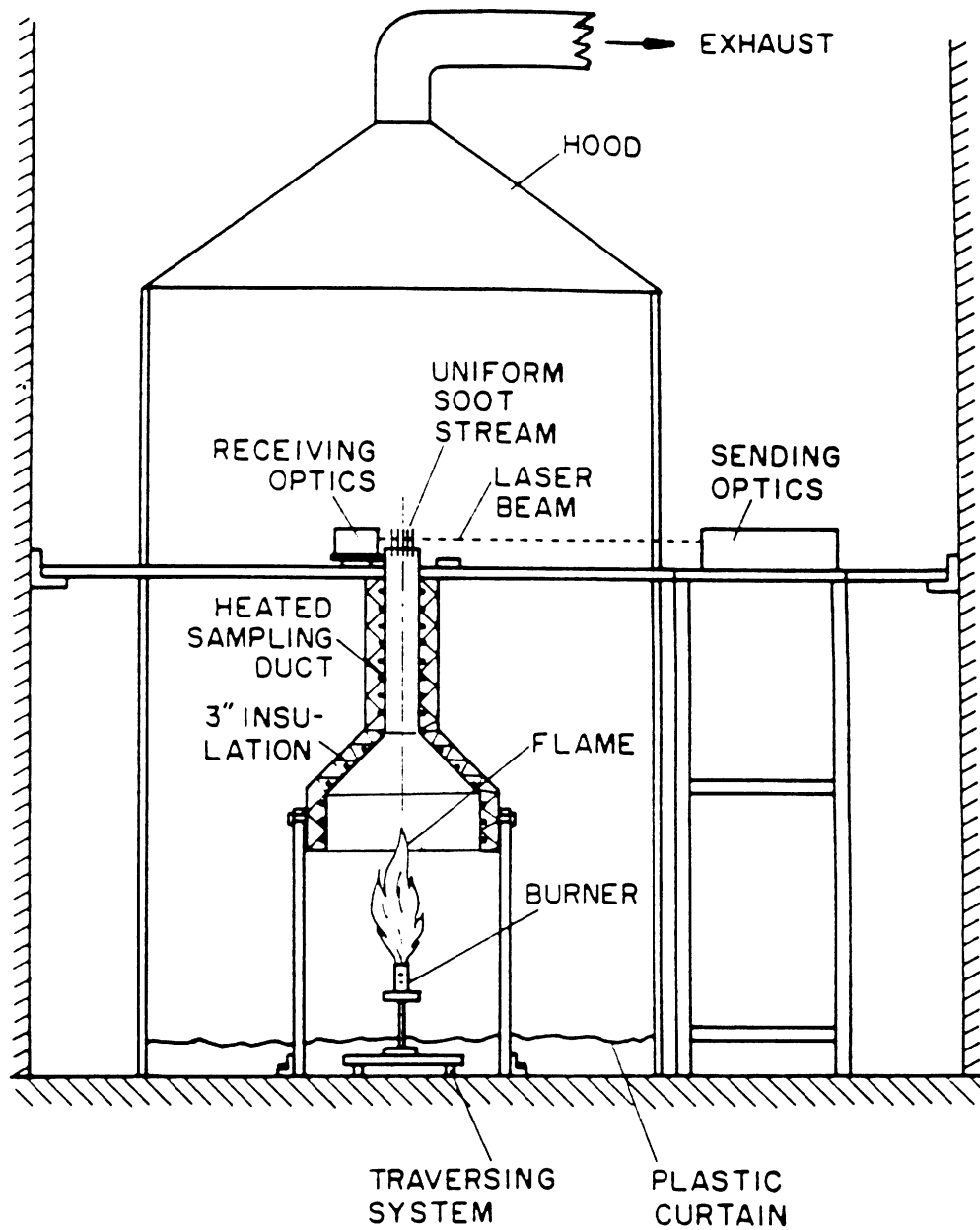


Fig. 2. Sketch of the buoyant turbulent diffusion flame apparatus.

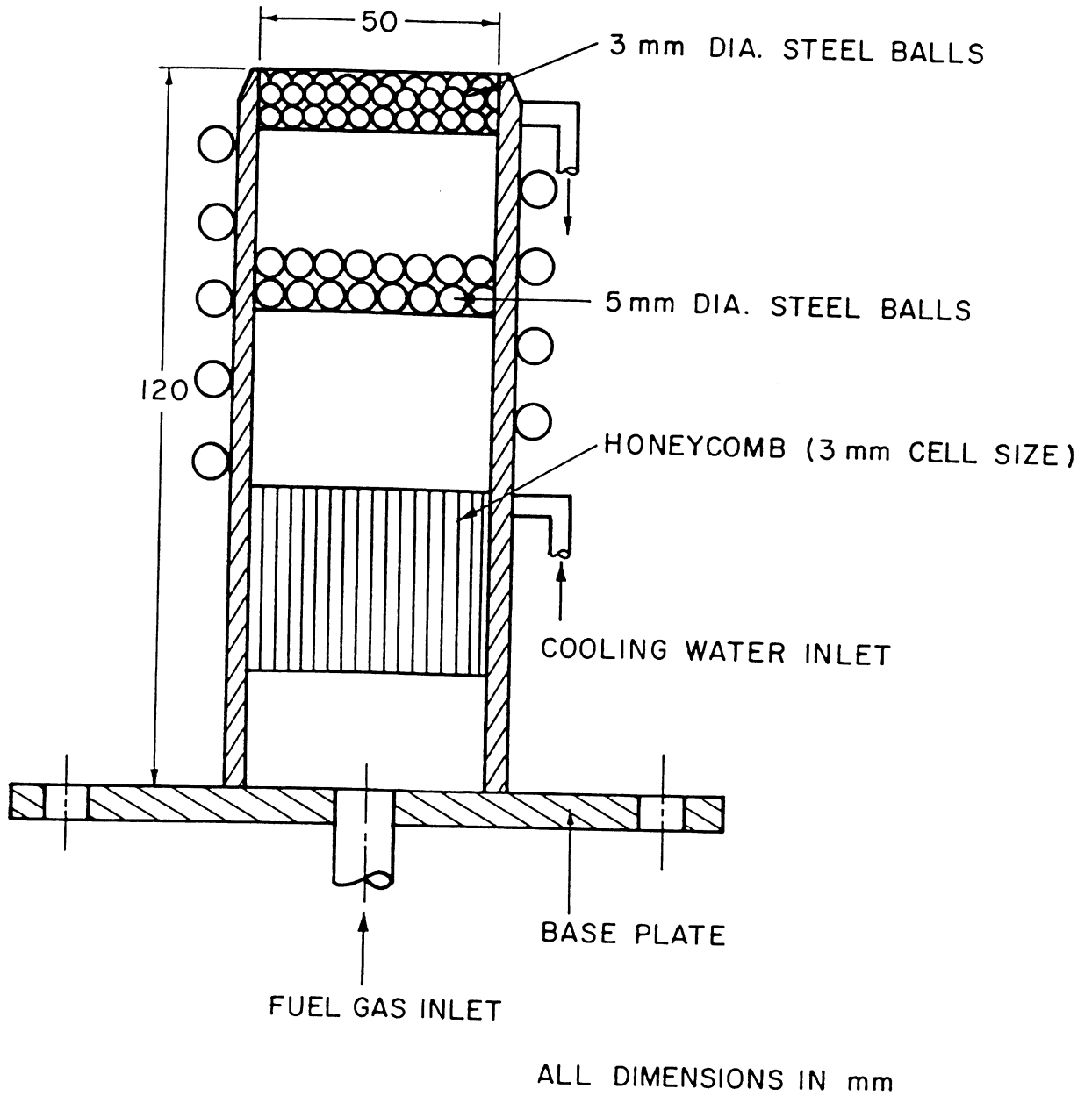
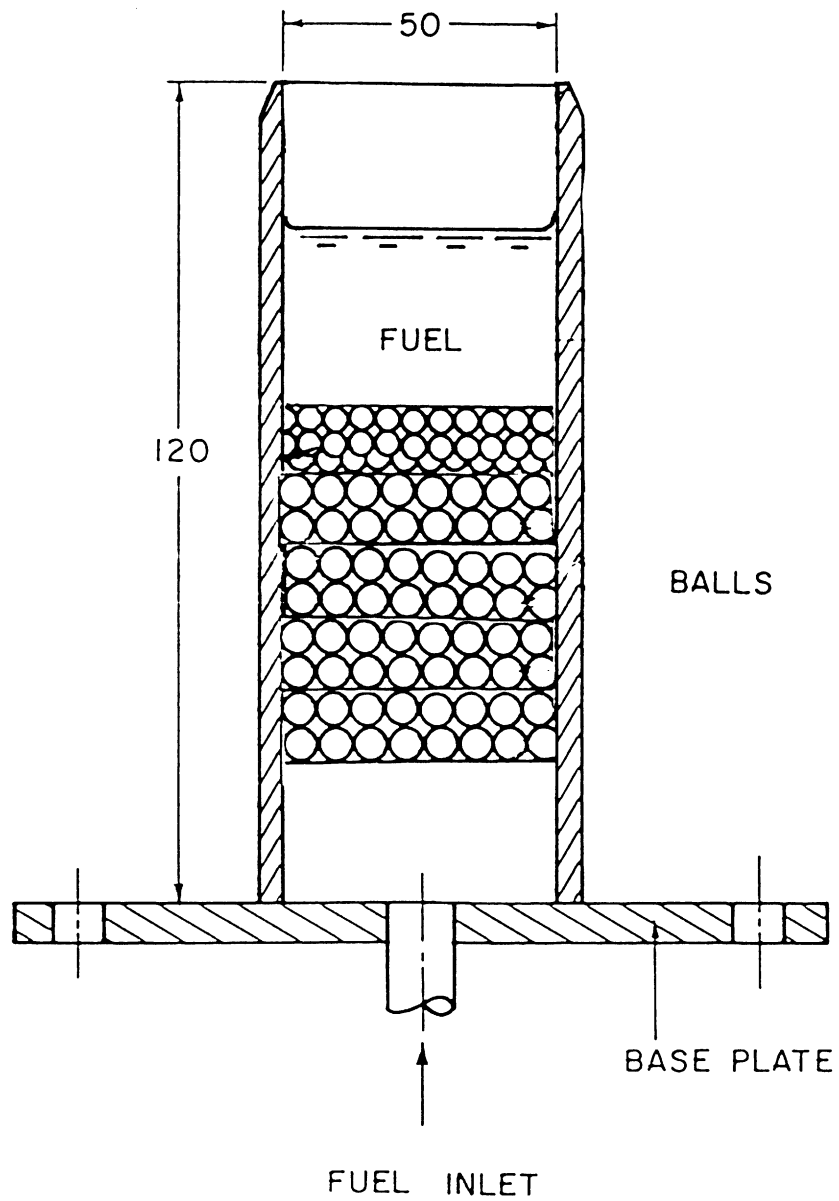


Fig. 3 Sketch of the gas-fueled diffusion flame burner.



ALL DIMENSIONS IN mm

Fig. 4 Sketch of the liquid-fueled diffusion flame burner.

With the exception of cyclohexane, soot structure, density and composition properties had been evaluated during earlier work (Köylü and Faeth, 1992). Measurements of the structure of cyclohexane had to be provided during the present investigation but this could be limited to measurements of primary soot particle diameter using thermophoretic sampling and TEM analysis in the usual manner (Köylü and Faeth, 1992). Other property variations among the various fuels for overfire soot were not very significant and were ignored.

Temperatures were measured along the optical path using a thermocouple probe. Temperatures of the mixture at the exit of duct were relatively low, 380-450 K, and were uniform across the duct exit as discussed earlier. Thus, conduction and radiation errors of these measurement were small, and experimental uncertainties (95% confidence) are estimated to be less than 10K.

The next step in measuring soot refractive indices using the present *in situ* method involved gravimetric determinations of the soot volume fractions in the region where extinction and scattering measurements were made. This involved a sampling train consisting of a sampling probe, a filter assembly, a flowmeter and a vacuum pump. The present flow is relatively uniform over a 150 mm diameter cross section; therefore, it was not necessary to employ a small probe for good spatial resolution. Thus, a 13 mm inside diameter water cooled sampling probe, aligned in the flow direction, was used. This probe was connected to a modified Gelman filter holder (Product 2220, in-line, 47mm) which in turn was connected through a flowmeter and valve to a vacuum pump. The flowmeter had a manometer at its inlet and was calibrated over the required range of inlet pressures using a wet test meter. A Gelman filter (Part no. 66143, 0.2  $\mu$ m, TF200, 47mm, PTFE membrane filter) was used in the filter holder to collect soot for a timed period while a second filter was used to mechanically collect any soot in the sampling line and the filter assembly. The mass of sampled soot was found by weighing the filters before and after sampling using an electronic balance. Then given the density of the soot, the mass of soot collected and the volume of gas sampled during the sampling period, the gravimetric soot volume fraction can be calculated in a straight-forward manner. Times of sampling were adjusted for these measurements in order to achieve experimental uncertainties (95% confidence) less than 6%.

The final results required for the *in situ* measurement of soot refractive indices are extinction and scattering measurements at the wavelengths of interest. The test arrangement for these measurements was identical to Köylü and Faeth (1994a). A sketch of the arrangement appears in Fig. 5 (on this figure, PR denotes polarization rotator, C denotes chopper, BS denotes beam splitter, L denotes lens, S denotes slit, P denotes polarization analyzer, F denotes narrow-band optical filter, NDF denotes neutral density filter, A denotes aperture, PMT denotes photomultiplier tube and D denotes photodetector). Although the figure indicates a laser as the source of illumination, various sources were used to cover the wavelength range as summarized in Table 1. The incident light beam was passed through a polarization rotator and a mechanical chopper (operating at 1250 Hz) before being focused at the centerline of the exhaust duct using a 1000 mm focal length lens. The collecting optics were mounted on a turntable surrounding the exhaust duct so that scattering angles,  $\theta=5-160$  deg, could be considered.

The collecting optics consisted of an 85 mm focal length lens, a dichroic sheet polarizer, a line filter (1nm bandwidth for the lasers, and 10nm bandwidth for the lamp), and a photomultiplier. The lens aperture defined a solid collection angle of 0.7 msr. Neutral density filters were used in the optical path to control the dynamic range of detection. The experimental area as well as the receiving optics were covered with black cloth to reduce optical noise from the room lighting and the flame. The test room also was

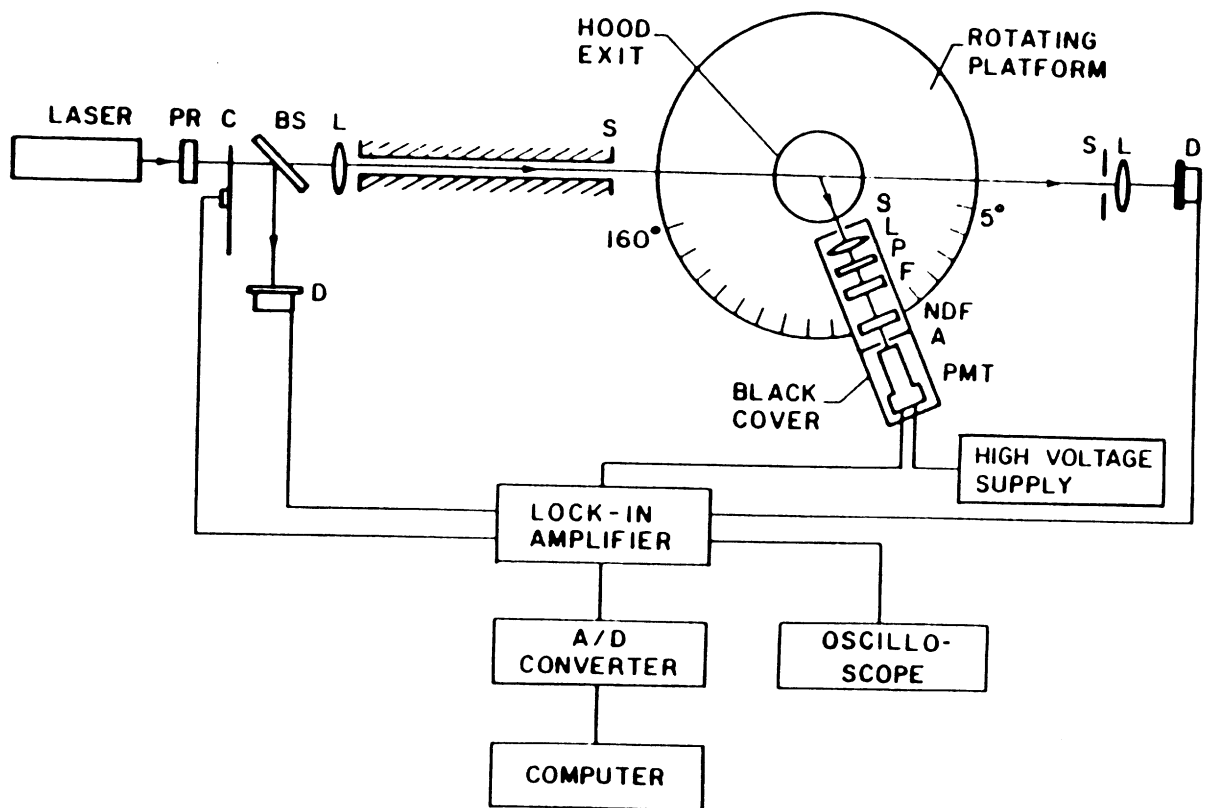


Fig. 5 Sketch of the radiation extinction and scattering instrument .

Table 1 Light Sources for the Measurements of Scattering from Soot

Wavelength (nm)	Light Source	Manufacturer and Model	Power
351.2	Argon-ion laser	Coherent Innova 90-4	100 mW
405.0	Mercury lamp	Oriel 6333	100 W
457.9	Argon-ion laser	Coherent-Innova 90-4	250 mW
488.0	Argon-ion laser	Coherent-Innova 90-4	1300 mW
514.5	Argon-ion laser	Coherent-Innova 90-4	1700 mW
632.8	He-Ne laser	Jodon, Model HN10GIR	28 mW
800.0	Diode laser	SDL-2360-P3	700 mW

windowless and provided dark-room conditions. The detector output passed through a lock-in amplifier and was stored on a computer sampling at 500Hz for 10s and averaging five sampling periods to achieve repeatability within 10%.

Except as noted, the angular light scattering system was calibrated by measuring Rayleigh scattering from propane gas. After correction for the reciprocal  $\sin \theta$  effect due to the geometry of the measuring volume, the vv and hh differential cross sections were within 5% of Rayleigh scattering predictions for  $\theta$  of 20-160 deg (see Fig. 6 for a typical scattering pattern of this type, at 514.5 nm). Absolute volumetric differential scattering cross sections of soot were found from ratios of the detector signal for soot and propane, after accounting for signal attenuation in the optical path, based on the propane and n-butane optical properties of Dyer (1979) and Rudder and Bach (1968). Total volumetric differential scattering cross sections were found by integrating the volumetric differential scattering cross sections over the whole spherical surface. This required extrapolation of the measurements to reach  $\theta = 0$  and  $180^\circ$ , however, uncertainties caused by the extrapolations were small due to the relatively small solid angles involved. The overall experimental uncertainties (95% confidence) of the angular and the total light scattering measurements were comparable and were estimated to be less than 20%, dominated by finite sampling times, the finite aperture of the detector and the angular uncertainty of the collecting optics; the corresponding uncertainties of the total extinction and absorption cross-sections are smaller, less than 5%, due to reduced effects of calibration uncertainties.

### 2.3 Theoretical Methods

Analysis of the scattering measurements to find soot optical properties was based on RDG-PFA theory as discussed by Wu et al. (1997). The main assumptions of RDG-PFA theory are as follows: individual primary particles satisfy the Rayleigh scattering approximation, soot aggregates satisfy the Rayleigh-Debye-Gans (RDG) scattering approximation, primary particles are spherical and monodisperse, primary particles just touch one another, the number of primary particles per aggregate satisfies a log-normal probability distribution function and the aggregates are mass fractal-like objects that satisfy the relationship given in Eq. (1) (Jullien and Botet, 1987). These approximations have proven to be satisfactory during past evaluations for a variety of conditions (Köylü and Faeth, 1992, 1994a,b,1996; Wu et al., 1997); nevertheless, they still were evaluated using present measurements before the theory was used to find soot optical properties.

The first step of the present calculations involved the determination of the mean number of primary particles per unit volume at the measurement location from the gravimetric measurement of soot volume fraction and the TEM measurement of primary particle diameter, as follows:

$$n_p = 6f_v / (\pi d_p^3) \quad (2)$$

Then, noting that  $\bar{Q}_a^a = \bar{Q}_e^a - \bar{Q}_s^a$ , so that  $\bar{Q}_a^a$  can be found from present measurements of  $\bar{Q}_e^a$  and  $\bar{Q}_s^a$ , the refractive index functions,  $E(m)$  and  $F(m)$  can be computed as follows:

$$E(m) = k^2 \bar{Q}_a^a / (4\pi x_p^3 n_p) \quad (3)$$

$$F(m) = k^2 (qd_p)^{D_f} \bar{Q}_{vv}^a (qd_p) / (k_f x_p^6 n_p) \quad (4)$$

where  $qd_p$  must be large enough so that scattering is in the large-angle (power-law) regime where Eq. (4) is appropriate. This requirement was established by noting the behavior of

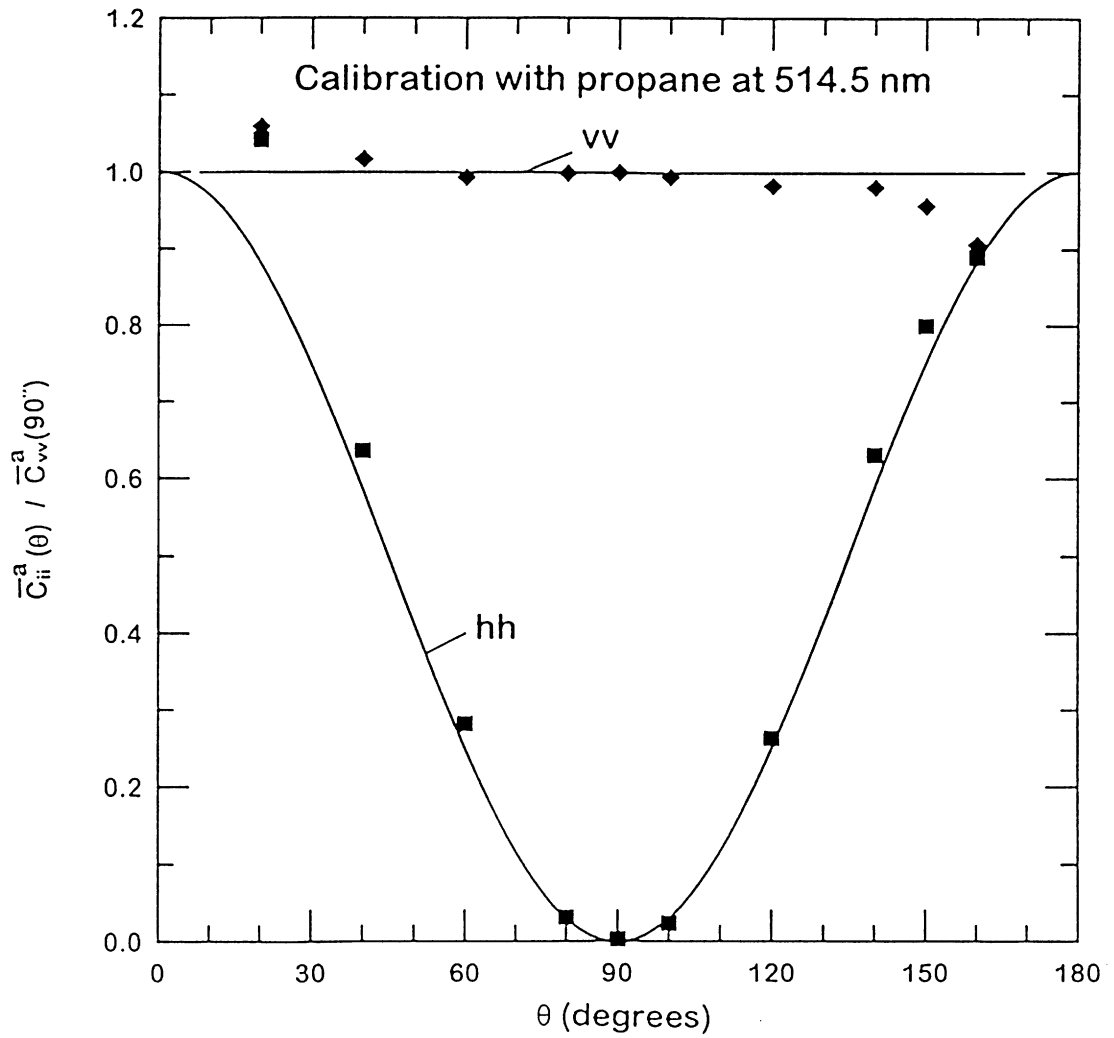


Fig. 6 Measured and predicted angular scattering patterns at 514.5 nm for Rayleigh scattering of gaseous propane.

RDG-PFA scattering at the limiting conditions of small-angle (Guinier) and large-angle (power-law) scattering, as follows:

$$\overline{Q}_{vv}^a(qd_p)/Q_{vv}^p = (\overline{N}^2/\overline{N})\exp(-q^2\overline{R}_g^2/3), \quad \text{Guinier regime} \quad (5)$$

$$\overline{Q}_{vv}^a(qd_p)/Q_{vv}^p = k_f(qd_p)^{-D_f}, \quad \text{power-law regime} \quad (6)$$

where the expression for  $\overline{R}_g^2$  in the Guinier regime can be found in Köylü and Faeth (1994a) while the value of  $k_f = 8.5$  was adopted from the recent determination of Köylü et al. (1995). The volumetric primary particle Rayleigh scattering cross section used to normalize Eqs. (5) and (6) is given by:

$$Q_{vv}^p = n_p x_p^6 F(m)/k^2 \quad (7)$$

From Eqs. (5) and (6) it can be seen that  $\overline{Q}_{vv}^a(qd_p)/Q_{vv}^p$  approaches the aggregate size moment,  $\overline{N}^2/\overline{N}$ , as  $qd_p$  approaches zero in the Guinier regime. It is also evident that  $\overline{Q}_{vv}^a(qd_p)/Q_{vv}^p$  provides a simple determination of soot fractal dimensions because  $D_f$  is the slope of this function in the power-law regime. Finally,  $E(m)$  and  $F(m)$  provide two nonlinear algebraic equations that can be solved to find the real and imaginary parts of the soot refractive indices.

The dimensionless extinction coefficient is a useful optical property that provides a simple relationship between extinction and soot volume fractions (Dobbins et al., 1994; Choi et al., 1995). This parameter was found for present test conditions by noting that properties were constant along the optical path used for extinction measurements, which implies (Choi et al., 1995):

$$k_{eR} = k_e(1+\rho_{sa}) = -\lambda \ln(I/I_o)/(Lf_v) \quad (8)$$

## 2.4 Results and Discussion

**Test Conditions.** Flame and soot properties at the test conditions are summarized in Table 2. The flames involved heat release rates of 2500-7400 W. The flames are ordered in the table in terms of decreasing propensity to soot, based on decreasing primary particle diameters at the measuring location. Primary particle diameters are in the range 30-51 nm and are in good agreement with earlier measurements of Köylü and Faeth (1992) for the soot emitted from hydrocarbon-fueled flames in the long residence time regime. The compositions of soot emitted several of the hydrocarbon-fueled flames in the long residence time regime were measured by Köylü (1992) and the results are summarized in the table; these results yield C/H, C/O and C/N atomic ratios of 8-17, 62-107 and 295-915, respectively. Typical aggregate dimensions were on the order of 1000-10000 nm, which is somewhat longer than the visible wavelengths; therefore, present measurements involved significant effects of scattering.

**Scattering Patterns.** RDG-PFA scattering theory was evaluated in order to justify the present approach to find soot refractive indices. The smallest wavelengths of the test range were a particular concern because values of  $x_p$  become large at these conditions which raises questions about the RDG scattering approximations (Faeth and Köylü, 1995). Thus, measured and predicted scattering patterns at the worst-case condition for the present

Table 2 Summary of test conditions for round buoyant turbulent diffusion flames in the long residence time regime.<sup>a</sup>

Fuel	Toluene	Benzene	Cyclohexane	Acetylene	Propylene	n-Heptane	Ethylene	Propane
Phase	liq.	liq.	liq.	gas	gas	liq.	gas	gas
Heat release rate (W)	2500	3400	5000	6160	6580	4100	5140	7400
Burner diameter (mm)	51	51	102	50	50	102	50	50
Gas temperature (K)	342	360	442	370	420	415	420	450
$d_p$ (nm)	51	50	49	47	41	35	32	30
$f_v$ (ppb)	471	379	94.6	476	247	38.5	44.6	27.8
$n_p$ (k-particles/mm <sup>3</sup> )	6780	5790	1584	8760	6840	1715	2600	1970
$D_f$ (-) <sup>b</sup>	1.79	1.77	1.81	1.74	1.79	1.79	1.78	1.78
N	526	552	----	417	460	260	467	364
Atomic ratios: <sup>c</sup>								
C/H	8.3	10.6	---	16.8	17.0	---	---	12.1
C/O	62.7	63.5	---	107.0	57.6	---	---	---
C/N	915	654	---	295	411	---	---	331

<sup>a</sup>Soot in the overfire region of buoyant turbulent diffusion flames in the long residence time regime. Soot densities (kg/m<sup>3</sup>): 1850 (liquids), 1870 (C<sub>2</sub>H<sub>2</sub>), 1850 (C<sub>3</sub>H<sub>6</sub>), 1930 (C<sub>2</sub>H<sub>4</sub>) and 1900 (C<sub>3</sub>H<sub>8</sub>).

<sup>b</sup>Effect of wavelength is small compared to experimental uncertainties.

<sup>c</sup>Measured by Köylü (1992).

test range (toluene soot at 351.2 nm which yields  $x_p = 0.46$ ) are illustrated in Fig. 7. Similar to past findings at longer wavelengths (Köylü and Faeth, 1994a), there is excellent agreement between measurements and predictions, justifying use of RDG-PFA scattering theory over the present test range. The scattering patterns in Fig. 7 exhibit strong scattering at small values of  $\theta$  in the Guinier regime which is not typical of Rayleigh scattering where  $\bar{Q}_{vv}^a$  would be relatively independent of  $\theta$ , highlighting the importance of considering RDG-PFA scattering theory when interpreting present measurements to find soot optical properties.

Another issue of importance is whether scattering from the present soot aggregates properly reaches the large angle (power-law) regime where Eq. (4), which is needed to close the present procedure to find refractive index properties, is valid. Initial results needed to establish this behavior can be obtained by comparing vv scattering patterns at the extremes of the test range, e.g., toluene soot at 351.2 nm in Fig. 7 and propane soot at 632.8 nm in Fig. 8. It is seen that the vv scattering patterns for these two conditions are identical for  $\theta \geq 30^\circ$ , clearly demonstrating extended power-law regimes over the present test range.

The results illustrated in Figs. 7 and 8 indicate relatively strong effects of depolarization which must be handled empirically when using RDG-PFA theory. This was done similar to Köylü and Faeth (1994a) by defining a depolarization ratio,  $\rho_v$ , as follows:

$$\bar{Q}_{hv}^a = \bar{Q}_{vh}^a = \bar{Q}_{hh}^a(90 \text{ deg}) = \rho_v \bar{Q}_{vv}^a(90 \text{ deg}) \quad (9)$$

This parameter is then used analogous to Rayleigh scattering theory, see Rudder and Bach (1968), to find values of  $\bar{Q}_{hh}^a(\theta)$  as follows:

$$\bar{Q}_{hh}^a(\theta) = [(1 - \rho_v) \cos^2 \theta + \rho_v] \bar{Q}_{vv}^a(\theta) \quad (10)$$

Present values of  $\rho_v$  are summarized as a function of fuel type and wavelength in Table 3, except for for conditions where scattering levels were too small for an accurate determination of  $\rho_v$ . Predictions illustrated in Figs. 7 and 8 show that the resulting correlation of  $\bar{Q}_{hh}^a(\theta)$  is excellent, similar to the predictions of  $\bar{Q}_{vv}^a(\theta)$ . The values of  $\bar{Q}_{hv}^a(\theta)$  and  $\bar{Q}_{vh}^a(\theta)$  illustrated in Fig. 8 also are in good agreement with the correlation of Eq. (9), except near the forward scattering direction where measured values increase and the vh and hv components are no longer equal. Experimental difficulties in the small angle region are thought to be responsible for this behavior because problems of alignment and cross polarization leakage are severe in the forward scattering direction where scattering levels are very high. Scattering behavior at other test conditions was similar to Figs. 7 and 8.

**Fractal Properties.** Evaluating whether present measurements properly reach the power-law regime, so that Eq. (4) can be used to find refractive indices, and exploiting these conditions to find fractal dimensions, can best be done by plotting  $\bar{Q}_{vv}^a(qd_p)/Q_{vv}^p$  as a function of the modulus of the scattering vector,  $qd_p$ , as suggested by Eq. (6). These results are illustrated for the gas-fueled flames at a wavelength of 632.8 nm in Fig. 9, however, behavior at other wavelengths and for the liquid-fueled flames is similar. The results shown in the figure include the measurements and predictions over the available ranges of  $qd_p$ , as well as the extrapolation of power-law behavior based on Eq. (6). As before, the substantial departure of scattering properties from Rayleigh scattering behavior

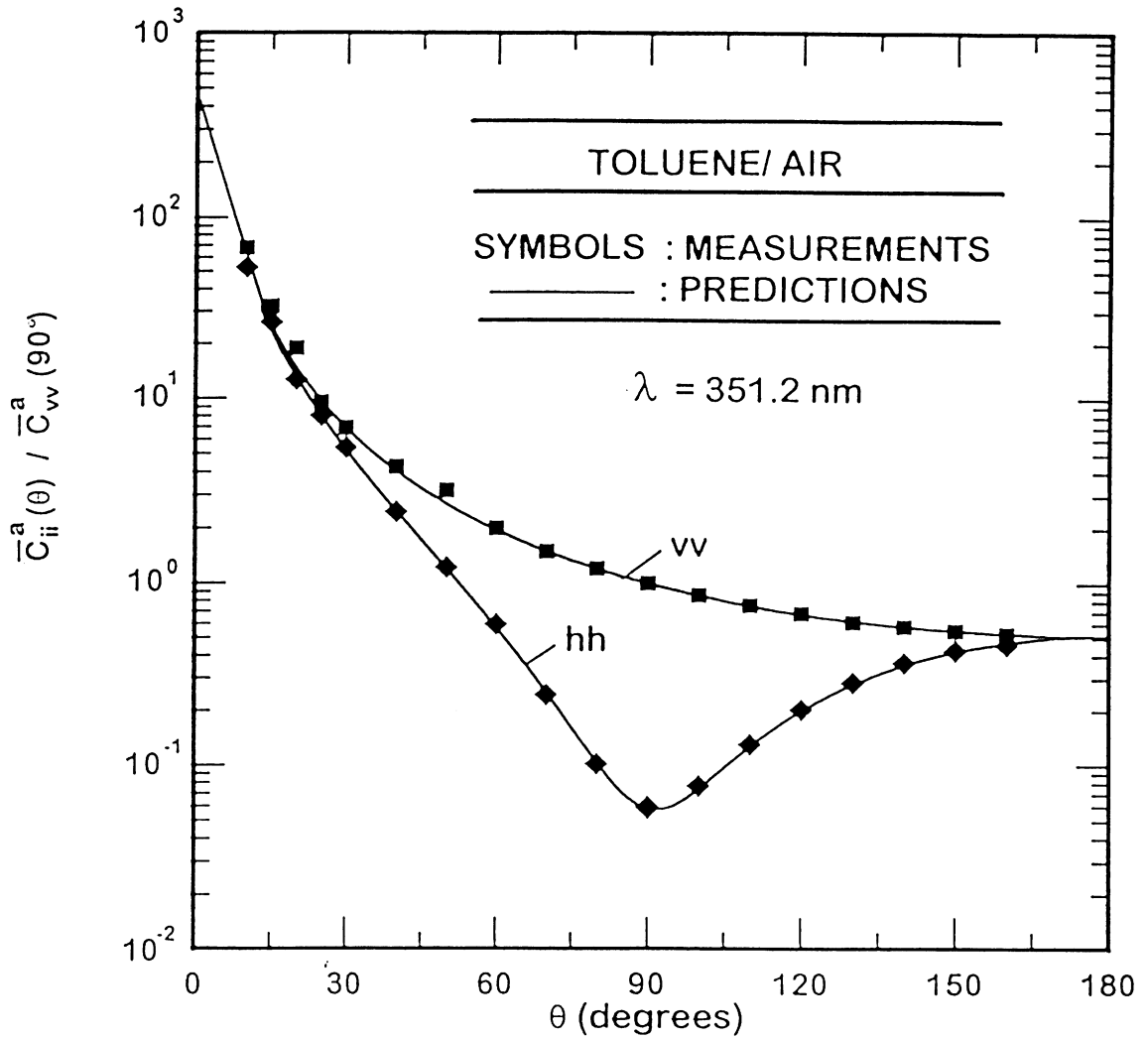


Fig. 7 Measured and predicted angular scattering patterns at 351.2 nm for overfiresoot aggregates in buoyant turbulent toluene/air diffusion flames.

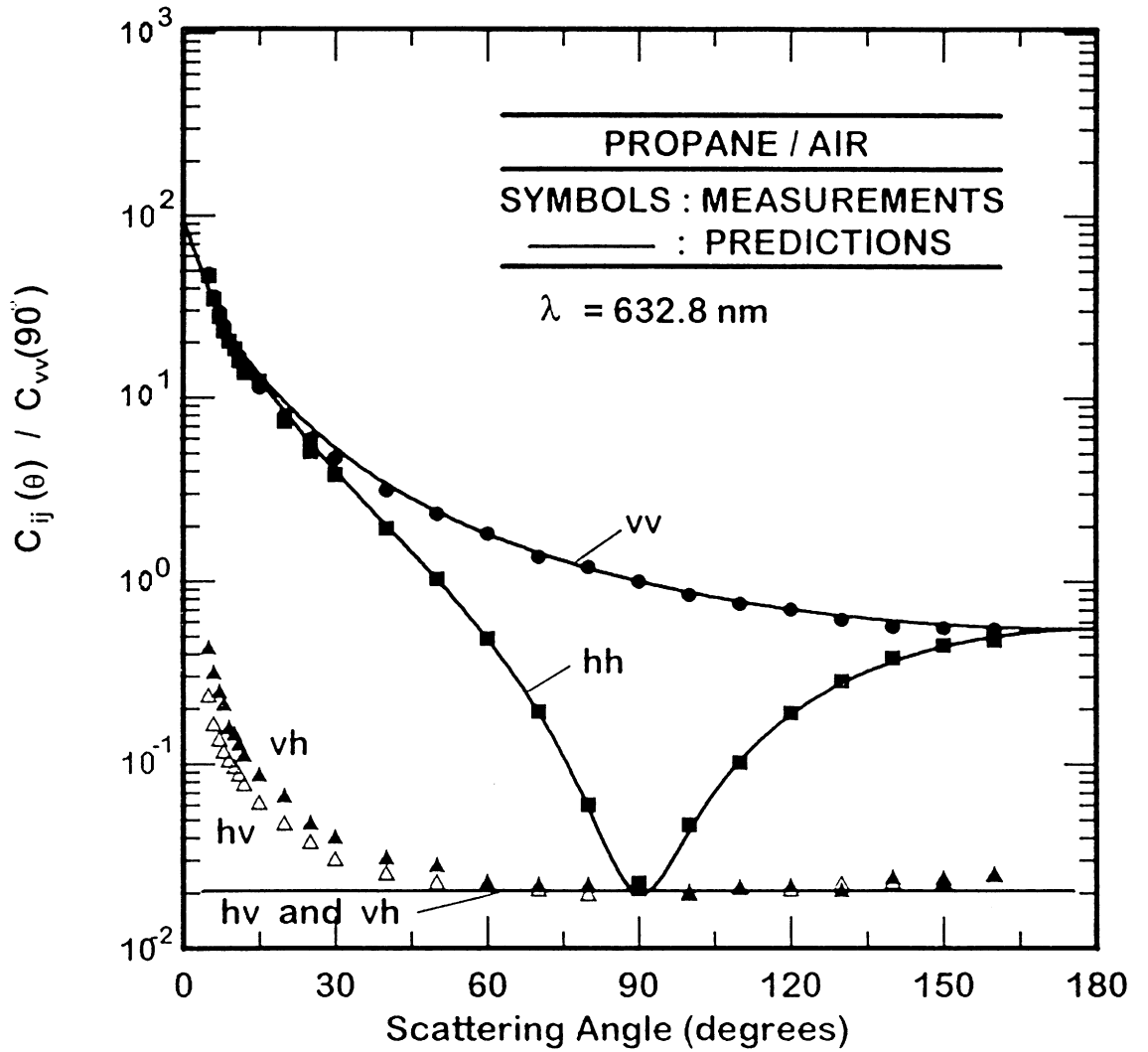


Fig. 8. Measured and predicted angular scattering patterns at 632.8 nm for overfire soot aggregates in buoyant turbulent propane/air diffusion flames.

Table 3 Summary of depolarization ratios: hydrocarbon-fueled flames<sup>a</sup>

Wavelength (nm)	Toluene	Benzene	Cyclohexane	Acetylene	Propylene	n-Heptane	Ethylene	Propane
351.2	0.058	0.047	0.036	0.070	0.065	0.033	0.056	0.044
405.0	0.047	0.048	0.034	0.055	0.042	---	0.041	0.038
457.9	0.049	0.049	0.048	---	---	0.039	---	---
488.0	0.032	0.044	0.034	0.042	0.033	0.034	0.026	0.022
514.5	0.035	0.027	0.031	0.041	0.030	0.034	0.023	0.020
632.8	0.026	0.022	0.030	0.038	0.028	0.025	0.022	0.019
800.0	0.038	0.037	0.048	0.032	---	---	---	---

<sup>a</sup>For overfire soot in buoyant turbulent diffusion flames in the long residence time regime, as summarized in Table 2.

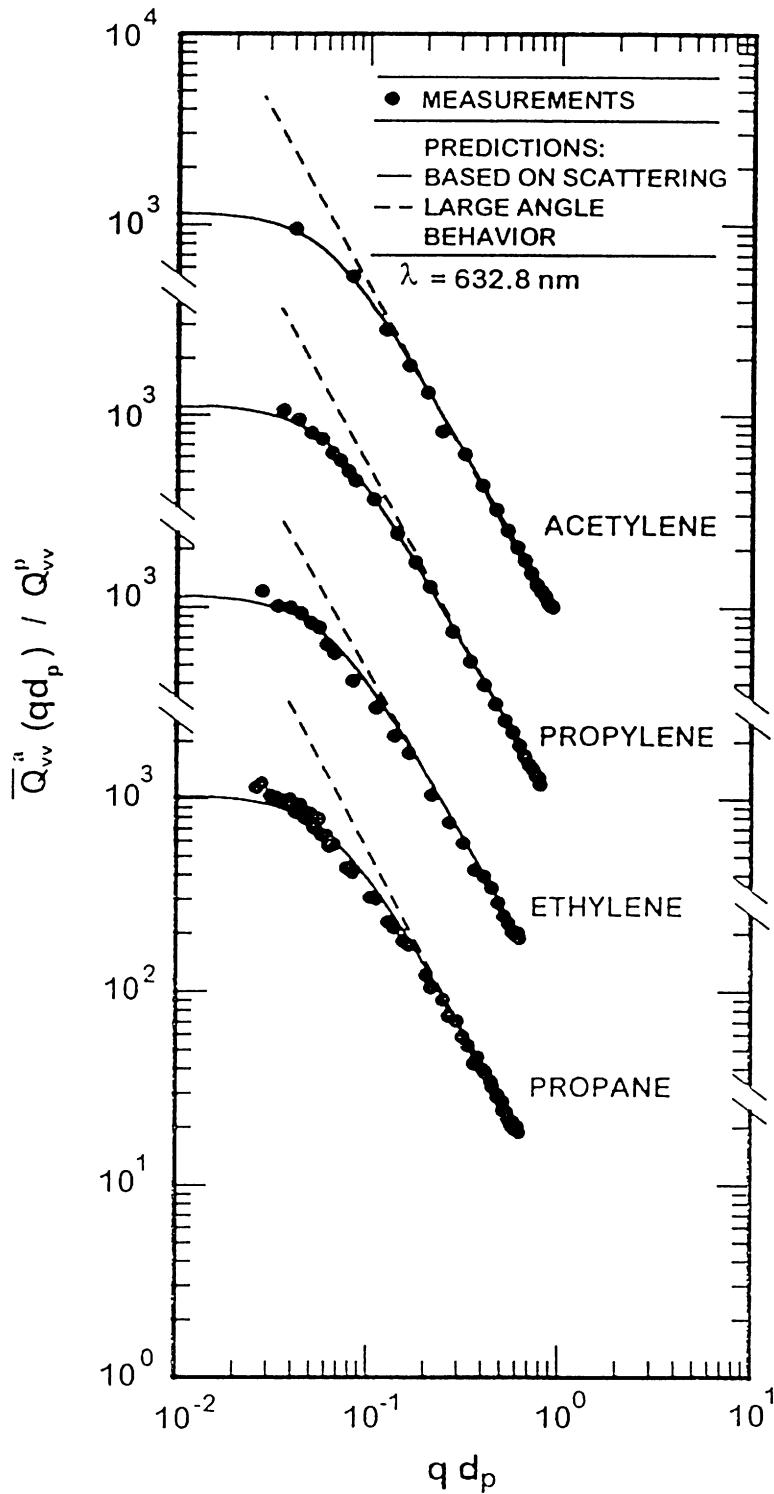


Fig. 9 Measured and predicted volumetric vv differential scattering cross-sections at 632.8 nm as functions of the modulus of the scattering vector for overfire soot aggregates in buoyant turbulent acetylene, propylene, ethylene and propane/air diffusion flames.

(where  $\bar{Q}_{vv}^a(qd_p)/Q_{vv}^p$  would be independent of  $qd_p$ ) is evident, with forward scattering 100-1000 times larger than back scattering for the present large soot aggregates. The measurements also clearly provide the extended power-law regime where scattering properties are represented by Eq. (6), e.g., roughly  $qd_p > 0.1$ , that is needed for the current *in situ* method to find soot refractive indices.

The measurements of  $\bar{Q}_{vv}^a(qd_p)/Q_{vv}^p$  in the power-law regime were used to compute fractal dimensions as discussed earlier. It was found that effects of wavelength were small, which is reasonable because fractal properties should only depend on the morphology of the soot aggregates. Thus, only mean values of  $D_f$  over the present wavelength range are summarized for each fuel in Table 2. Clearly, the variation of  $D_f$  with fuel type is not very significant either, yielding a mean value of  $D_f = 1.78$  with a standard deviation of 0.02. These results are in good agreement with earlier determinations of fractal dimensions due to Köylü and Faeth (1994a) for the same soot, and with measurements of other soot in flame environments, see Köylü and Faeth (1994a), Faeth and Köylü (1995) and references cited therein. This universality of soot fractal dimensions in flames is very helpful for exploiting RDG-PFA scattering theory to find soot properties from scattering measurements and to estimate continuum radiation properties.

**Refractive Index Properties.** Results thus far have shown that RDG-PFA theory performs reasonably well for present conditions, that present scattering measurements are consistent with earlier measurements for the same soot, that present fractal dimensions are in good agreement with earlier work, and that present scattering measurements at large angles ( $qd_p > 0.1$ ) are within the power-law regime. Based on these findings, Eqs. (2)-(8) were used to compute soot optical properties from the present measurements, after adopting  $k_f = 8.5$  from Köylü et al. (1995) as mentioned earlier. Results at 800.0 nm, for the gas-fueled flames and at 405.0 and 800.0 nm for the liquid-fueled flames were exceptions, because signal-to-noise ratios at these wavelengths were too low to provide adequate absolute calibrations of scattering levels based on Rayleigh scattering from propane. For gas-fueled flames at 800 nm, the fact that  $\rho_{sa}$  was nearly independent of wavelength for each fuel was exploited in order to obtain absolute scattering levels at 800.0 nm from the extinction measurements for each fuel (Wu et al., 1997). A similar approximation for  $\rho_{sa}$  for the liquid fuels was not satisfied; therefore, only  $k_{eR}$  was found at 405.0 and 800.0 nm for these fuels.

The refractive index functions,  $E(m)$  and  $F(m)$ , actually are the most important refractive index properties needed to use RDG-PFA theory and will be considered first. Present measurements of these functions for both gas- and liquid-fueled flames are plotted as a function of wavelength in Fig. 10. The values of  $E(m)$  are relatively independent of the fuel type and wavelength over the entire test range, increasing only slightly with increasing wavelength. This universality is rather convenient because it implies a simple relationship between absorption and soot concentrations through Eq. (3). In contrast,  $F(m)$  progressively increases with increasing wavelength for both the liquid- and gas-fueled flames; this behavior helps maintain scattering levels nearly constant with increasing wavelength in spite of the fundamental reduction of scattering with increasing wavelength expected for RDG-PFA scattering (Faeth and Köylü, 1995).

The resulting real and imaginary parts of the refractive indices of soot from the present measurements are plotted as a function of wavelength, with fuel type as a parameter, in Fig. 11. Combining all factors, the experimental uncertainties of the real and imaginary parts of the refractive indices of soot (95% confidence) are estimated to be less than 20%. although outlying points are currently being rechecked to improve the results.

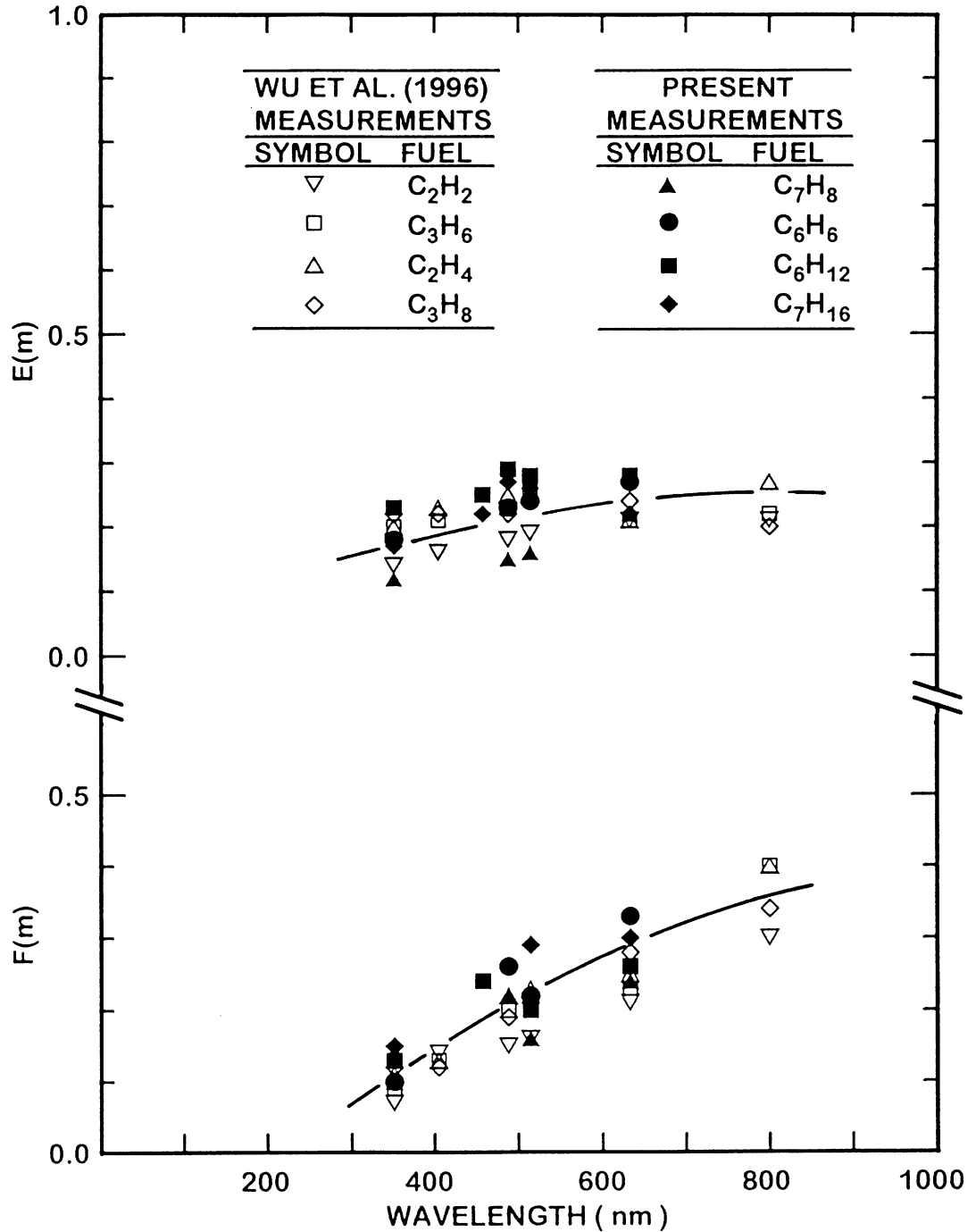


Fig. 10 Measured refractive index functions,  $E(m)$  and  $F(m)$ , in the visible (350-800 nm) for overfire soot aggregates in buoyant, turbulent diffusion flames.

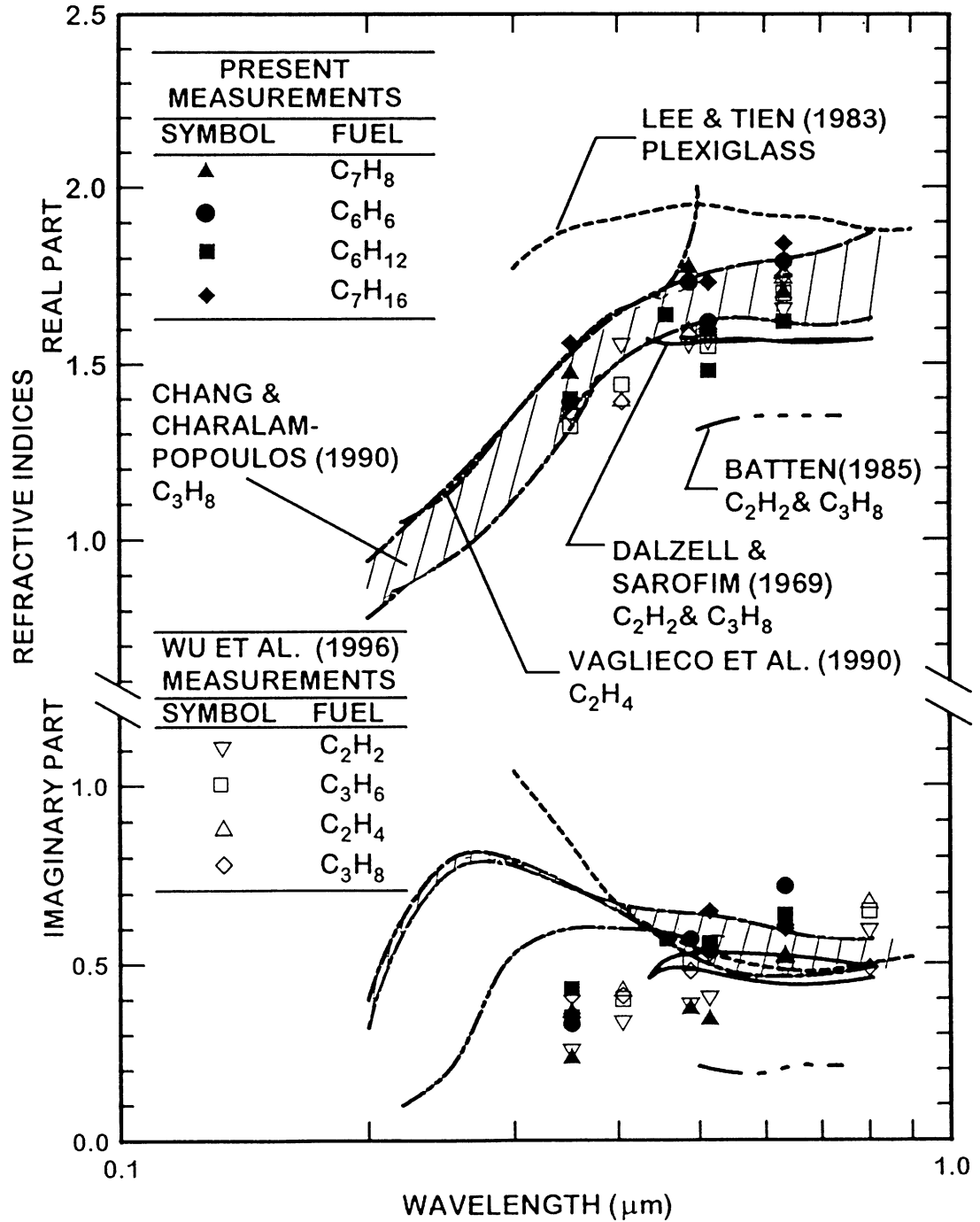


Fig. 11 Measured refractive indices of soot in the near ultraviolet and visible portions of the spectrum. Measurements of Battin (1985), Chang and Charalampopoulos (1990), Dalzell and Sarofim (1969), Wu et al. (1997) and the present study.

Similar to the refractive index functions, the refractive indices themselves exhibit relatively small effects of fuel type within present experimental uncertainties. This behavior generally agrees with past observations of soot refractive indices in diffusion flames, see Wu et al (1997), Köylü and Faeth (1996), Faeth and Köylü (1995), Dalzell and Sarofim (1969) and references cited therein.

Several earlier measurements of soot refractive indices are illustrated in Fig. 11 for comparison with the present results. These measurements include the classical *ex situ* reflectometry measurements for soot in the fuel-lean region of acetylene/air and propane/air diffusion flames due to Dalzell and Sarofim (1969), the *ex situ* measurements for soot in the fuel-lean region of acetylene/air and propane/air diffusion flames due to Batten (1985), the *in situ* measurements for soot in the fuel-lean region of plexiglass/air diffusion flames due to Lee and Tien (1983), the *in situ* measurements for soot in the post-flame region of fuel-rich premixed propane/air flames due to Chang and Charalampopoulos (1990), the *in situ* measurements for soot in the post-flame region of fuel-rich premixed ethylene/air flames due to Vaglieco et al. (1990), and the *in situ* measurements for soot emitted from gas-fueled buoyant turbulent diffusion flames due to Wu et al. (1997). It should be noted that the *ex situ* measurements of Dalzell and Sarofim (1969) have been criticized by Lee and Tien (1980) for potential problems of soot property changes due to soot collection and sample preparation, and by Felske et al. (1984) for potential problems of diffuse scattering for reflectometry measurements due to surface roughness. On the other hand, the measurements of Lee and Tien (1983), Batten (1985), Chang and Charalampopoulos (1990) and Vaglieco et al. (1990) can be criticized as noted earlier, because they all involve questionable models for the optical properties of soot, some involve questionable soot transport properties in cases where dynamic scattering measurements are used to estimate soot aggregate properties, and some involve questionable approximations associated with either Drude-Lorentz dispersion models or Kramers-Krönig causality relationships used to close the procedure to find soot refractive indices. Finally, Chang and Charalampopoulos (1990) observe variations of soot refractive indices with increasing residence time in the post-flame region of premixed flames, attributed to an effect of soot aging (or annealing) in a high temperature environment, so that their results are indicated by a band.

The present measurements of soot refractive indices illustrated in Fig. 11 are seen to agree best with the findings of Dalzell and Sarofim (1969), as noted earlier, similar to the findings of Wu et al. (1997) and Köylü and Faeth (1994a,1996), in spite of past criticism of this methodology. Nevertheless, reasons for this behavior and for the discrepancies among various investigators, as well as adequate definition of effects of fuel type, wavelength, flame conditions and residence time, clearly merit additional study. Present refractive indices are seen to progressively increase as wavelength is increased. This behavior acts to reduce the variation of extinction, absorption and scattering cross sections with increasing wavelength as discussed earlier. Finally, present measurements of soot refractive indices do not exhibit an effect of resonance in the near ultra-violet range of the spectrum that is seen for graphite; instead, the present soot refractive indices progressively decrease as the near ultra-violet is approached, which tends to agree with recent observations of Vaglieco et al. (1990) and Wu et al. (1997) who observed little evidence of a resonance near the uv. Naturally, this behavior implies problems for some past determinations of soot refractive indices where the presence of resonance conditions is assumed, by analogy with graphite, when either Drude-Lorentz dispersion relations or Kramers-Krönig causality relationships were developed.

The standard deviations of  $E(m)$  and  $F(m)$  over all fuel types at each wavelength are less than 25%, while the corresponding standard deviations of  $n$  and  $\kappa$  over all fuel types at each wavelength are less than 6 and 30%. These values are comparable to experimental uncertainties so that effects of fuel type cannot be identified within statistical significance

from present results, as noted earlier. Thus, these properties are summarized as a function of wavelength, after averaging over all the gas-fueled flames in Table 4, over all the liquid-fueled flames in Table 5, and over the combined gas- and liquid-fueled flames in Table 6. The relatively close agreement between the overall averages and the widely-quoted refractive index values of  $n = 1.56$  and  $\kappa = 0.57$  at 514.5 nm from Dalzell and Sarofim (1969) is quite evident.

Dimensionless Extinction Coefficients. Present determinations of the dimensionless extinction coefficient,  $k_{eR}$ , also did not exhibit significant variations with fuel type over the present test range. Thus, values of  $k_{eR}$  for gas-fueled, liquid-fueled and for hydrocarbon-fueled flames are summarized as a function of wavelength in Tables 4 to 6. These results are also plotted, grouping findings for gas-fueled and liquid-fueled flames, in Fig. 12. The experimental uncertainties of present measurements of  $k_{eR}$  (95% confidence) are estimated to be less than 20%. Present values of  $k_{eR}$  are in the range 4.6-7.0 and really do not exhibit significant variations with wavelength and fuel type. This behavior comes about due to fortuitous cancellation of effects of scattering, wavelength and refractive index variations. Values of  $k_{eR}$  averaged over the gas- and liquid-fueled flames are summarized as a function of wavelength in Tables 4 and 5 respectively, yielding average values of  $k_{eR}$  for these fuel types of 5.1 and 6.2, respectively. Then averaging over all fuels and wavelengths yields a mean value of  $k_{eR}$  of 5.7 with a standard deviation of 0.7.

Other measurements of  $k_{eR}$  are plotted in Fig. 12 for comparison with the present measurements. This includes measurements for soot in the fuel-lean region of crude-oil/air diffusion flames due to Dobbins et al. (1994), and measurements for soot in the post-flame region of premixed fuel-rich acetylene/air flames due to Choi et al. (1995). Clearly, the results of Dobbins et al. (1994), with values of  $k_{eR}$  in the range 8.1-9.4, and the results of Choi et al. (1995) with a mean value of  $k_{eR} = 8.6$ , with a standard deviation of 0.5, are significantly larger than present results in Tables 4-6 for reasons that still must be explained.

## Conclusions

The fractal and optical properties of soot were studied experimentally, considering soot within the overfire region of gas- and liquid-fueled buoyant turbulent diffusion flames in the long residence time regime, where soot properties are independent of position in the overfire region and residence time for a particular fuel. The investigation was limited to soot in flames fueled by toluene, benzene, cyclohexane, acetylene, propylene, n-heptane, ethylene and propane and burning in still air, and to wavelengths in the visible (350-800 nm). The main conclusions of the study are as follows:

1. Present soot refractive indices did not vary significantly with fuel type and were in reasonably good agreement with earlier measurements for similar conditions due to Dalzell and Sarofim (1969).
2. Present soot refractive indices did not exhibit an approach to a resonance condition in the near uv that is observed for graphite; instead, refractive indices declined continuously as the near uv was approached, similar to the observations of Vaglieco et al. (1990) for amorphous carbon and soot.
3. Present dimensionless extinction coefficients were relatively independent of fuel type and wavelength, yielding an average value of 5.7 and a standard deviation of 0.7; however, these values are significantly smaller than values in the range 8.1-9.4

Table 4 Soot optical properties: gas-fueled flames<sup>a</sup>

Wavelength (nm)	E(m)	F(m)	n	$\kappa$	$k_{eR}$
351.2	0.19	0.10	1.36	0.35	4.6
405.0	0.21	0.13	1.45	0.40	5.0
488.0	0.22	0.19	1.58	0.48	5.4
514.5	0.24	0.20	1.58	0.51	5.3
632.8	0.22	0.24	1.71	0.53	5.4
800.0 <sup>b</sup>	0.23	0.36	----	0.65	5.1

<sup>a</sup>Average values for overfire soot within buoyant turbulent diffusion flames in the long residence time regime. Measurements consider flames fueled with acetylene, propylene, ethylene and propane burning in still air as summarized in Table 2.

<sup>b</sup>Results at this wavelength were found from extrapolated values of  $\rho_{sa}$ .

Table 5 Soot optical properties: liquid-fueled flames<sup>a</sup>

Wavelength (nm)	E(m)	F(m)	n	$\kappa$	$k_{eR}$
351.2	0.18	0.12	1.70	0.28	4.6
405.0	----	----	----	----	6.0
457.9	0.27	0.15	1.87	0.36	6.3
488.0	0.24	0.29	1.53	0.61	7.0
514.5	0.24	0.22	1.69	0.52	6.4
632.8	0.25	0.28	1.59	0.62	5.8
800.0	---	----	----	----	6.3

<sup>a</sup>Average values for overfire soot within buoyant turbulent diffusion flames in the long residence time regime. Measurements consider flames fueled with toluene, benzene, cyclohexane and n-heptane burning in still air as summarized in Table 2.

Table 6 Soot optical properties: hydrocarbon-fueled flames<sup>a</sup>

Wavelength (nm)	E(m)	F(m)	n	$\kappa$	$k_{cR}$ <sup>d</sup>
351.2	0.18	0.11	1.53	0.32	5.0
405.0 <sup>b</sup>	0.21	0.13	1.45	0.40	5.5
457.9 <sup>c</sup>	0.27	0.15	1.87	0.36	6.3
488.0	0.23	0.24	1.56	0.55	6.2
514.5	0.24	0.21	1.64	0.52	5.9
632.8	0.24	0.26	1.65	0.58	5.6
800.0 <sup>b</sup>	0.23	0.36	----	0.65	5.7

<sup>a</sup>Averaged values for overfire soot within gas-fueled flames from Wu et al. (1997) and within liquid-fueled flames from the present study.

<sup>b</sup>Results for E(m), F(m), n and  $\kappa$  only for gas-fueled flames from Wu et al. (1997).

<sup>c</sup>Results only for liquid-fueled flames from the present study.

<sup>d</sup>Average of all values equals. 5.7.

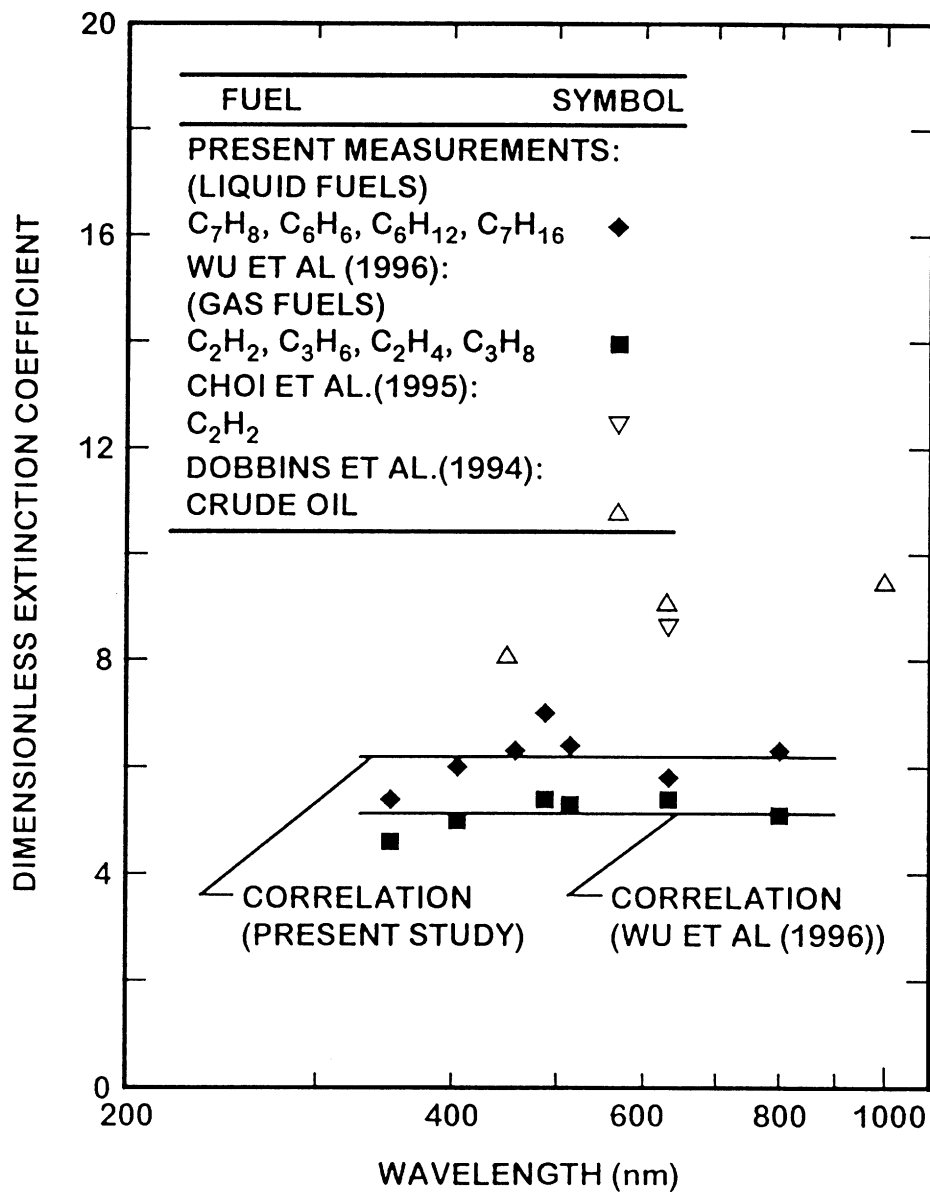


Fig. 12 Measured dimensionless extinction coefficients in the visible portion of the spectrum. Measurements of Choi et al. (1995), Dobbins et al. (1994), Wu et al. (1997) and the present study.

reported by Dobbins et al. (1994) and Choi et al. (1995) for reasons that still must be explained.

4. Present fractal dimensions were relatively independent of fuel type and wavelength, yielding an average value of 1.78 and a standard deviation of 0.02, which is in reasonably good agreement with the measurements of Köylü and Faeth (1994a) for similar soot emitted from buoyant turbulent diffusion flames in the long residence time regime.
5. The approximate RDG-PFA scattering theory agreed with present measurements within experimental uncertainties; this represents a severe test of the approximate theory because primary particle optical diameters reached values up to 0.46, which represent the largest values considered thus far.

### **3. Buoyant Turbulent Plumes**

#### **3.1 Introduction**

The structure and mixing properties of buoyant turbulent plumes in still and unstratified environments is an important fundamental problem that has attracted significant attention since the classical study of Rouse et al. (1952). However, recent work has highlighted the need for a better fundamental understanding of buoyant turbulent plumes in order to address effects of turbulence/radiation interactions (Faeth et al., 1989, 1990; Panchapakesan and Lumley, 1993; Pivovarov et al., 1992; Ramaprian and Chandrasekhara, 1985, 1989; Shabbir and Taulbee, 1990). Thus, the overall objective of this phase of the investigation is to complete new measurements of the properties of buoyant turbulent plumes and to exploit the information to improve both understanding and modeling of these flows. The fully-developed region (where effects of the source have been lost and the properties of the flow become self-preserving) is emphasized because these conditions simplify both theoretical considerations and the interpretation of measurements (Tennekes and Lumley, 1972), even though few practical plumes reach a self-preserving state.

Present considerations have been limited to the structure and mixing properties of buoyant turbulent plumes in still and unstratified environments. Self-preserving buoyant turbulent plumes are reached when streamwise distances from the plume source are large compared to the characteristic source size (the source diameter for round plumes or the source width for plane plumes) as a measure of conditions where effects of soot source disturbances have been lost, and the Morton length scale as a measure of conditions where effects of buoyancy are dominant. Such conditions generally imply that mixture fractions are small,  $f \ll 1$ , and yield the rather simple scaling relationships for mean mixture fractions and streamwise velocities that are summarized in Table 7, as discussed by Morton (1959) and Morton et al. (1956). Results presented in the table include scaling for both round and plane (line) plumes both of which have been of interest since the work of Rouse et al. (1952) and are being addressed during the present study.

Several reviews of turbulent plumes have appeared (Kotsovinos, 1985; List, 1982; Papanicolaou and List, 1987, 1988); therefore, the following discussion of past studies will be brief. The earliest work emphasized the development of similarity relationships for flow properties within fully-developed (self-preserving) buoyant turbulent plumes (Rouse et al., 1952). Subsequently, many workers reported observations of properties at self-

Table 7 Scaling of self-preserving turbulent plumes<sup>a</sup>

Parameter	Formula
<b>Round Plume:</b>	
Source momentum flux	$M_o = (\pi/4)d^2 u_o^2$
Source buoyancy flux	$B_o = (\pi/4)d^2 u_o g   \rho_o - \rho_\infty   / \rho_\infty$
Morton length scale	$\ell_M = M_o^{3/4} / B_o^{1/2}$
Velocity scaling	$U(r/(x-x_o)) = \bar{u}((x-x_o)/B_o^{1/3})$
Mixture-fraction scaling	$F(r/(x-x_o)) = \bar{f}gB_o^{2/3} (x-x_o)^{5/3}   \rho_o - \rho_\infty   / \rho_o$
<b>Plane Plume:</b>	
Source momentum flux	$M_o = bu_o^2$
Source buoyancy flux	$M_o = bu_o g   \rho_o - \rho_\infty   / \rho_\infty$
Morton length scale	$\ell_M = M_o / B_o^{2/3}$
Velocity scaling	$U(y/(x-x_o)) = \bar{u} / B_o^{1/3}$
Mixture-fraction scaling	$F(y/(x-x_o)) = \bar{f}gB_o^{-2/3} (x-x_o)   \rho_o - \rho_\infty   / \rho_o$

<sup>a</sup>Assuming  $f \ll 1$  so that  $\ln \rho_{f \rightarrow 0} = | \rho_o - \rho_\infty | / \rho_o$ .

preserving conditions, however, these determinations generally were not in good agreement (George et al., 1977; Kotsovinos, 1985; Mizushima et al., 1979; Ogino et al., 1980; Papanicolaou and List, 1987, 1988; Papantoniou and List, 1989; Peterson and Bayazitoglu, 1992; Shabbir and George, 1992; Zimin and Frik, 1977). Papanicolaou and List (1987, 1988) attribute these discrepancies mainly to problems of fully reaching self-preserving conditions, with conventional experimental uncertainties serving as a contributing factor.

Initial measurements of self-preserving plumes in this laboratory involved consideration of round buoyant turbulent plumes. A sketch of the experimental apparatus used for these measurements appears in Fig. 13. The arrangement consisted of a large outer enclosure ( $3000 \times 3000 \times 3400$  mm high) containing the test plume within a smaller screened enclosure ( $1100 \times 3200$  mm high). The plumes involved source flows of gaseous carbon dioxide and sulfur hexafluoride in still air at atmospheric pressure and temperature, in order to provide a straightforward specification of the plume buoyancy flux. This yielded negatively buoyant, downward flowing plumes that were removed at the bottom of the enclosure using a blower and bypass system. The inner enclosure and the position of the source could be traversed to accommodate rigidly-mounted instrumentation. Mixture fractions were measured using laser-induced iodine fluorescence (LIF), velocities were measured using laser-velocimetry (LV), and combined mixture-fraction/velocity statistics were measured using combined LIF/LV, similar to Lai et al. (1988) and Lai and Faeth (1987a,b).

The development of transitional round buoyant turbulent plumes toward self-preserving conditions can be seen from the radial profiles of mean mixture fractions illustrated in Fig. 14. In this case, the scaling parameters of Table 7 are used so that the ordinate is equal to  $F(r/(x-x_0))$ . The radial mean mixture fraction profiles exhibit progressive narrowing, with scaled values at the axis progressively increasing, as the streamwise distance increases. However, self-preserving conditions are observed within experimental uncertainties for  $12 \leq (x-x_0)/\ell_M \leq 43$  and  $87 \leq (x-x_0)/d \leq 151$  (the upper end of these ranges represents the largest streamwise distance considered during present measurements). This regime corresponds to plume Reynolds numbers of 2500-4200 which are reasonably large for unconfined turbulent flows.

Corresponding radial profiles of mixture fraction fluctuations in round turbulent plumes are plotted in Fig. 15 for two sources. Near the source the profiles are broad and exhibit a dip near the axis, similar to the behavior of nonbuoyant jets (Becker et al., 1967; Panchapakesan and Lumley, 1993; Papanicolaou and List, 1987,1988). However, both the flow width and the magnitude of the dip near the axis gradually decrease as streamwise distance is increased. Eventually, self-preserving behavior is obtained within the same range of streamwise distances where mean mixture fractions were self-preserving. Analogous to mean mixture fractions, most earlier measurements of r.m.s. mixture fraction fluctuations are representative of transitional plumes with broader profiles and smaller values of  $(f'/f)_c$ . For example, Papanicolaou and List (1987,1988), Shabbir and George (1992) and George et al. (1977) find  $(f'/f)_c = 0.40$ , rather than 0.45 for the present measurements.

Measurements of velocities within the round turbulent plumes were limited to the self-preserving region, namely  $(x-x_0)/d \geq 87$  and  $(x-x_0)/\ell_M \geq 12$ . Profiles of mean streamwise velocities are illustrated in Fig. 16 which is plotted in terms of the scaling

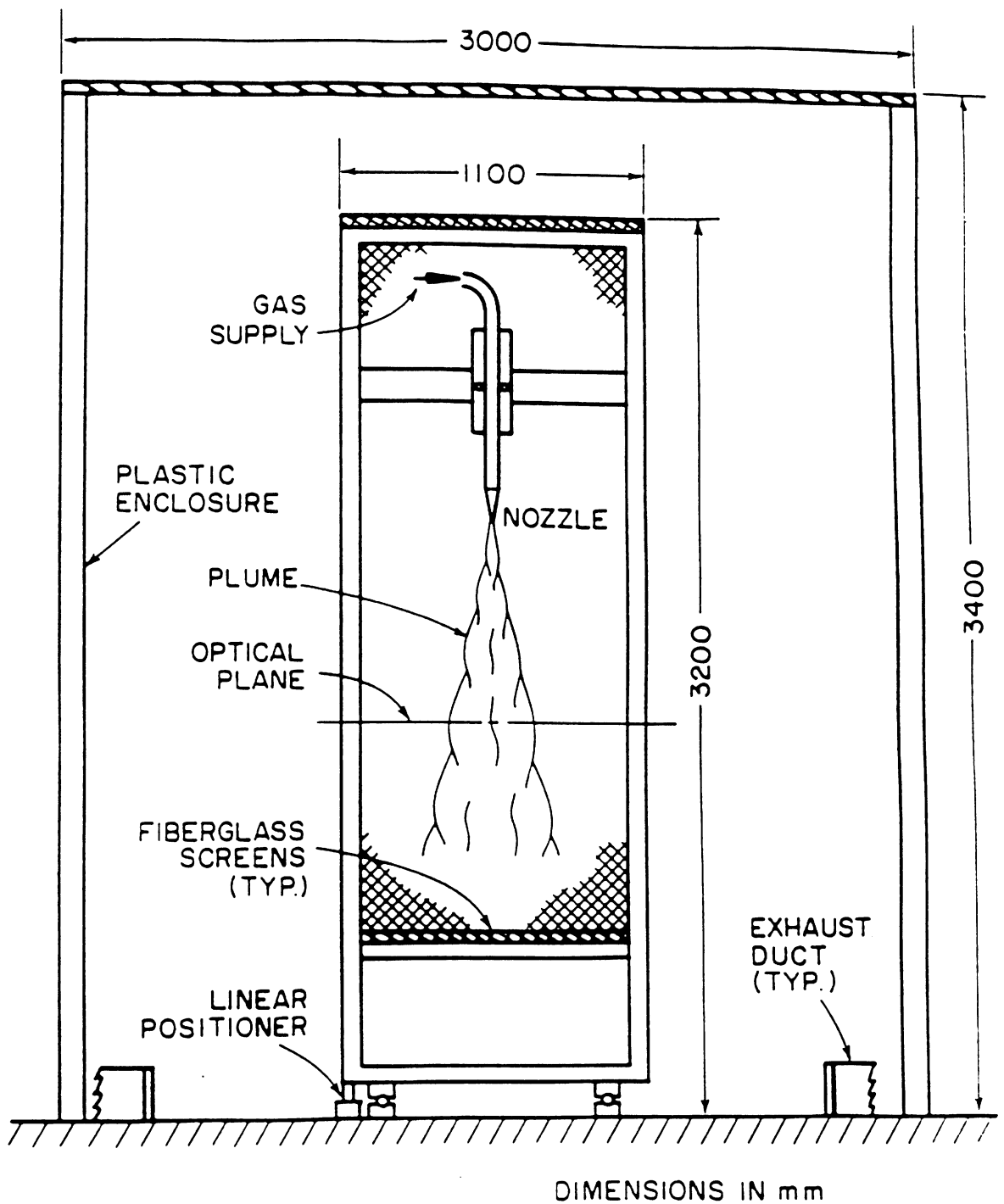


Fig. 13 Sketch of the round buoyant turbulent plume test apparatus.

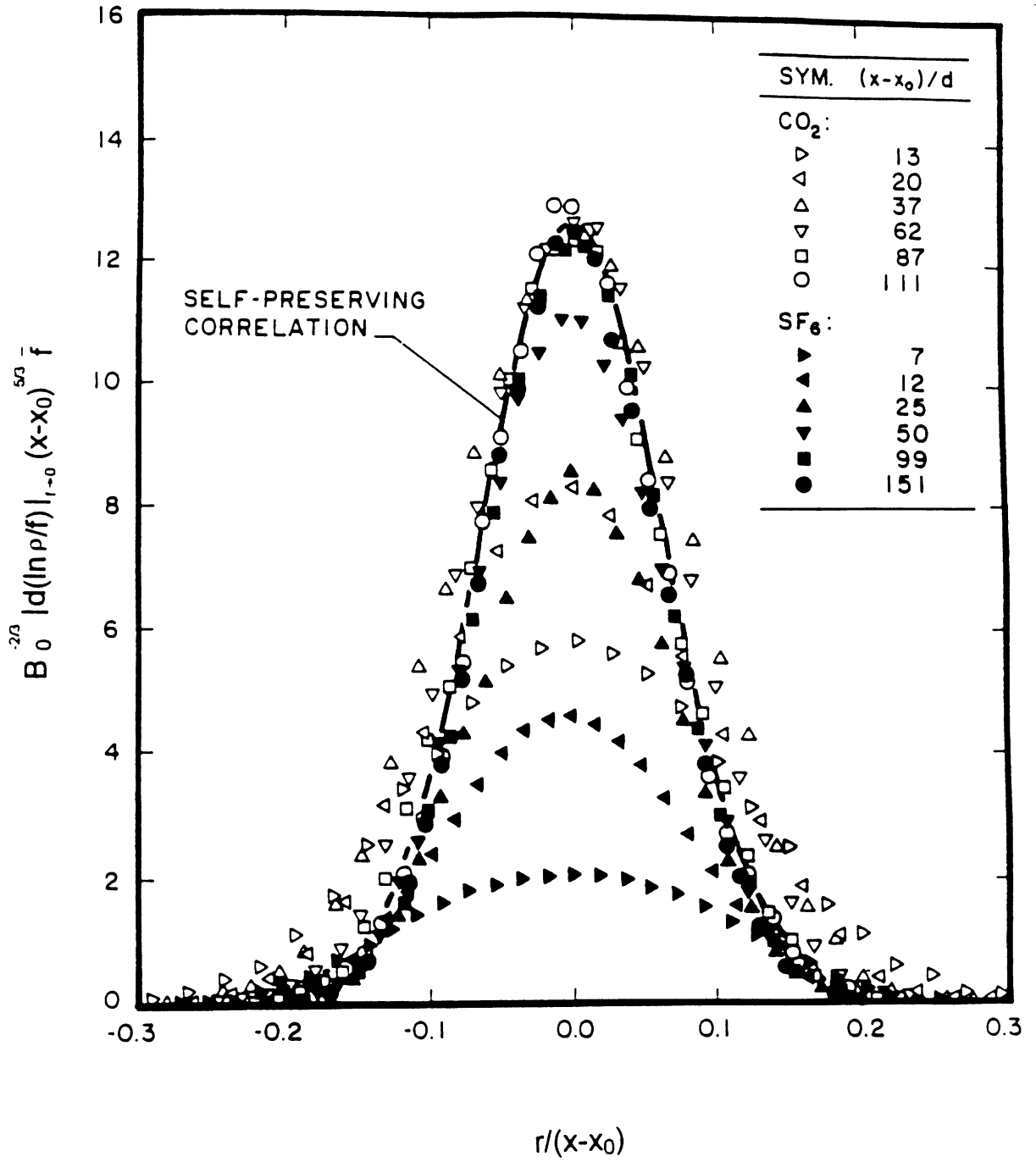


Fig. 14 Radial profiles of mean mixture fractions in round buoyant turbulent plumes. From Dai et al. (1994).

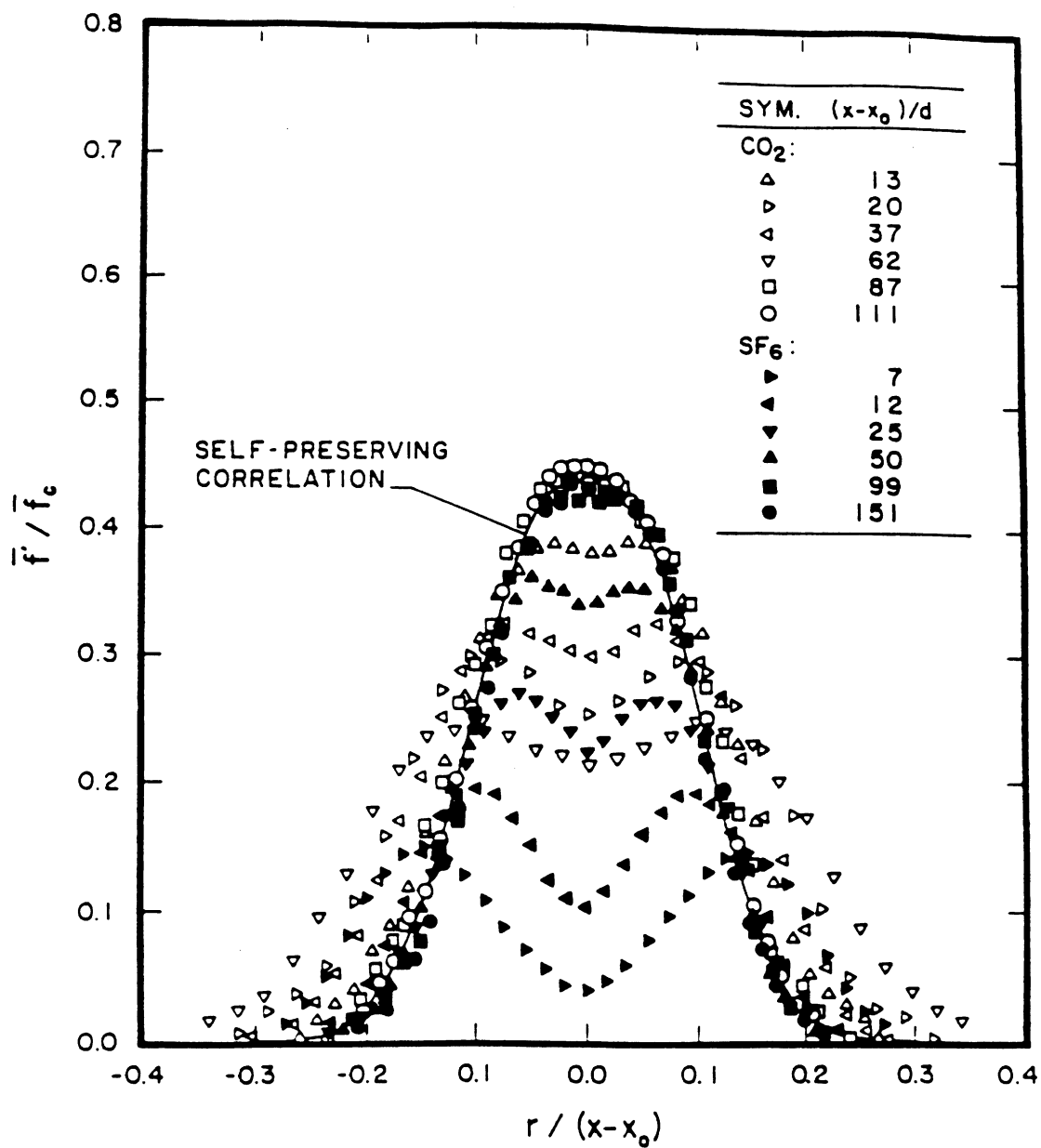


Fig. 15 Radial profiles of r.m.s. mixture fraction fluctuations in round buoyant turbulent plumes. From Dai et al. (1994).

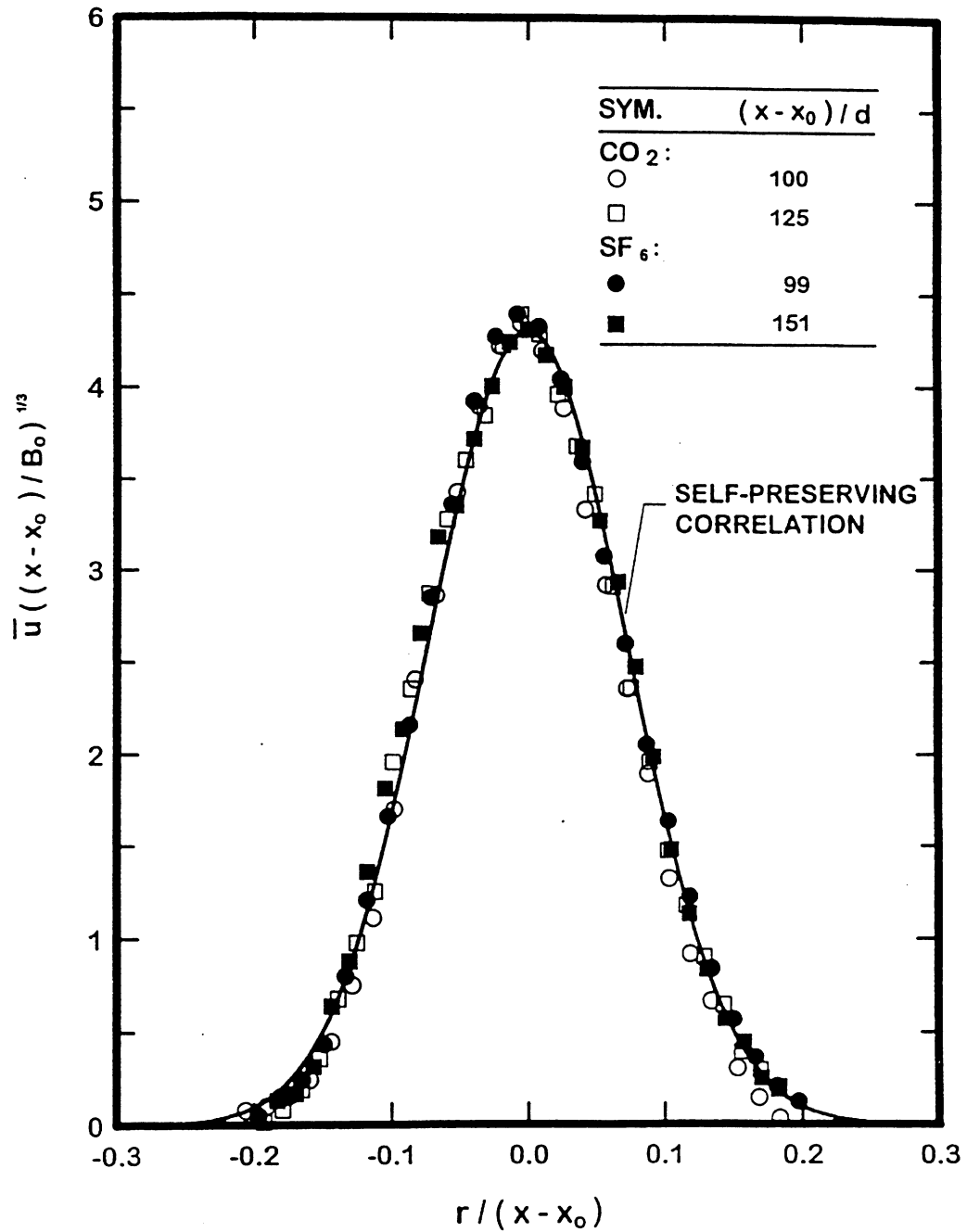


Fig. 16 Radial profiles of mean streamwise velocities in self-preserving round buoyant turbulent plumes. From Dai et al. (1995a).

parameters for self-preserving round turbulent plumes so that the ordinate is equal to  $U(r/(x-x_0))$ . It is evident that  $U(r/(x-x_0))$  is a universal function within experimental uncertainties over the range of the measurements, as anticipated for self-preserving flow.

Radial profiles of velocity fluctuations within round turbulent plumes for the self-preserving region of the two sources are illustrated in Fig. 17. It is seen that the profiles are universal within experimental uncertainties over the range of conditions considered. The presence of the dip near the axis is similar to nonbuoyant jets and is expected because turbulence production is reduced near the axis due to symmetry (Panchapekesan and Lumley, 1993). Nevertheless, this behavior differs from mixture fraction fluctuations, illustrated in Fig. 15, and is another unusual feature of buoyant turbulent plumes. Finally, while the velocity fluctuations are nearly isotropic near the edge of the plumes, streamwise velocity fluctuations are roughly 25% larger than the cross-stream velocity fluctuations near the axis.

Numerous other turbulence properties were measured for the self-preserving region of round buoyant turbulent flows, and subsequently exploited to evaluate typical models of the process, see Dai and Faeth (1996) and Dai et al. (1994,1995a,b). These results suggested that contemporary turbulence models provided reasonably successful predictions of the mean properties of these simple self-preserving boundary-layer like flows (which is not very surprising, in fact, simple mixing length, etc. models would do just as well) but that most predictions of turbulence properties using these models were not satisfactory. This is unfortunate because predictions of turbulence properties play a central role in estimating important properties of unwanted fires, such as turbulence/radiation interactions, while the potential to estimate these properties represents the main value added by turbulence models compared to simpler methods such as mixing length models.

Given results for self-preserving round turbulent plumes, the current research is beginning to address flows more directly relevant to the flows encountered during unwanted fires within structures. This work has begun with consideration of self-preserving plane turbulent plumes, which is the simplest configuration similar to plane turbulent flows along surfaces but without the immediate complications due to the presence of a surface. This flow is also of great fundamental importance as the classical buoyant turbulent plane or line plume, analogous to the classical nonbuoyant turbulent plane or line jet.

Turbulent plane plumes are problematical due to the difficulties of assuring a proper two-dimensional flow while avoiding ambient disturbances and potential unstable interactions between the plume and its surroundings. Dealing with these problems requires sources having large aspect ratios to insure two-dimensionality as well as extensive test programs to establish that effects of the surroundings on the flow are small. As a result, there have been far fewer studies of plane turbulent plumes than round turbulent plumes. Thus, past studies of plane turbulent plumes are limited to the classical initial study of Rouse et al. (1952) for plumes in gases, and the subsequent studies of Kotsovinos (1977), Kotsovinos and List (1977) and Ramaprian and Chandrasekhara (1985,1989) for plumes in liquids. All these studies sought results in the self-preserving region of the flow, however, whether this was achieved is questionable because measurements were limited to the region relatively close to the source,  $(x-x_0)/b < 60$ . In particular, past work for round turbulent plumes in this laboratory suggests that streamwise distances greater than  $(x-x_0)/d > 80$  are needed to achieve self-preserving behavior. Past measurements involve other

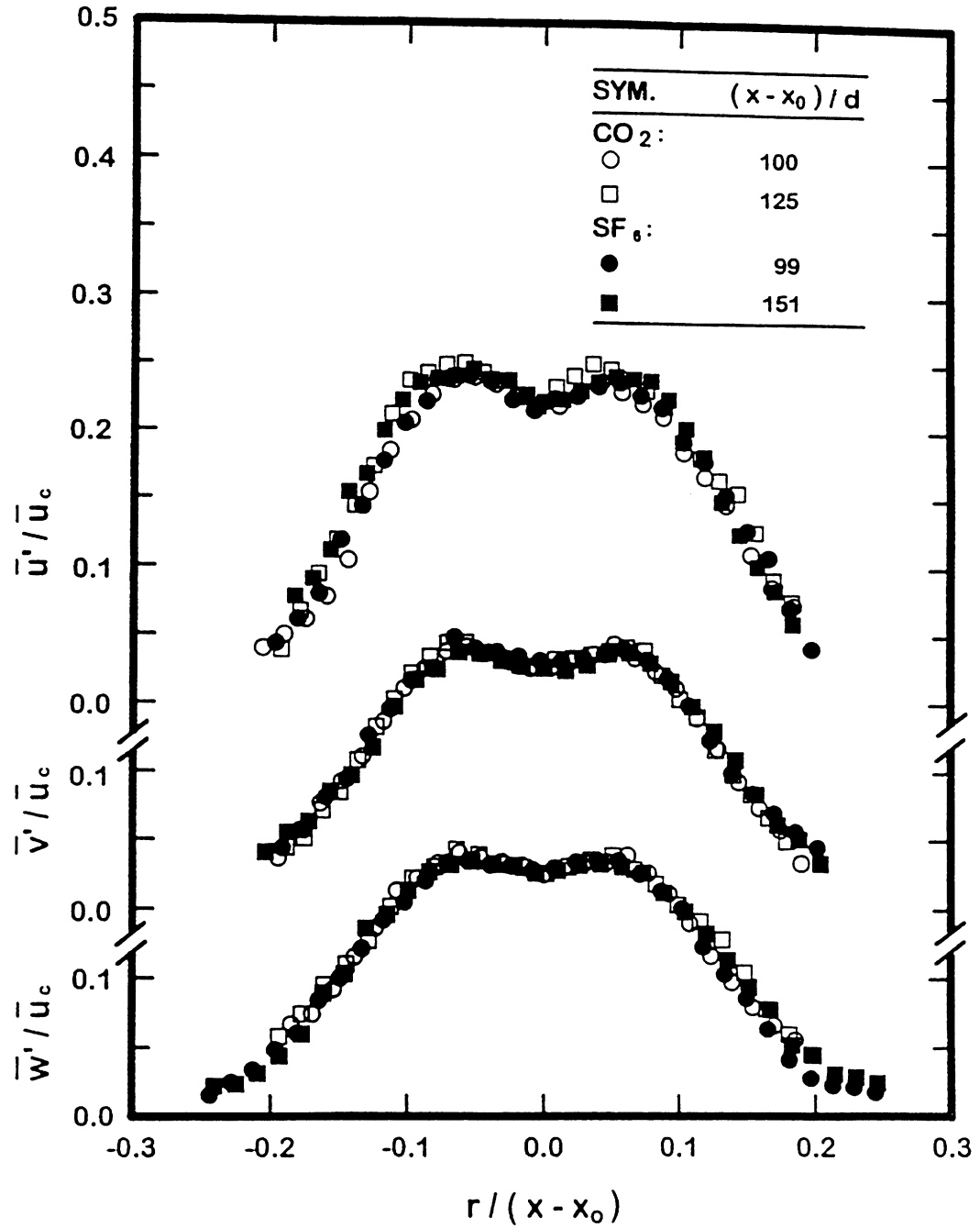


Fig. 17 Radial profiles of r.m.s. velocity fluctuations in self-preserving round buoyant turbulent plumes. From Dai et al. (1995a).

difficulties as well: the source properties of Rouse et al. (1952) are difficult to characterize so that estimates of  $(x-x_0)/b$  for these flows cannot be made, the aspect ratios of the plane liquid plumes are disturbingly small in the region where measurements were made, the liquid plumes involved thermal sources where effects of parasitic heat losses near the source are difficult to define, measurements of turbulent properties are very limited for all these flows and are nonexistent for the gaseous plumes that are of greatest interest for unwanted fire applications.

Thus, based on these observations, the objectives of this phase of the investigation are as follows:

- (i) To complete measurements of mean and fluctuating properties within plane turbulent plumes, emphasizing self-preserving conditions where complications due to source disturbances have been lost.
- (ii) To exploit the new measurements in order to develop and evaluate theories of buoyant turbulent flow, considering classical similarity theories as well as more complex turbulence modeling procedures that are needed to treat turbulence/radiation, turbulence/buoyancy and other turbulence interactions in practical fire environments.

During this report period, the main emphasis has been on developing the experimental apparatus, initiating measurements of mixture fraction properties, and seeking to establish self-preserving behavior for plane turbulent plumes. In the following, experimental methods and results will be discussed in turn before ending with the conclusions that can be made thus far. It should be emphasized, however, that present measurements are still considered to be preliminary, pending completion of the full test program that is currently in progress.

### **3.2 Experimental Methods.**

Apparatus. A sketch of the free plane buoyant turbulent plume apparatus appears in Fig. 18. It has been necessary to make significant changes in the experimental approach compared to the round plumes, in order to accommodate the much larger flow and entrainment rates of plane plumes, compared with round plumes. In fact, the problems of developing the plane plume apparatus far exceeded our anticipation in spite of extensive experience with experimental studies of plane plumes along surfaces in this laboratory (Grella and Faeth, 1975; Lai and Faeth, 1987a,b; Lai et al., 1986; Liburdy and Faeth, 1978; Liburdy et al., 1979). The main difficulties involved assuring reasonable aspect ratios for two-dimensional flows while controlling effects of room disturbances and confinement.

The present turbulent plane plume apparatus involves mixtures of air and helium as the source fluid, yielding positively buoyant upward flowing plumes. This step was necessary to control costs of gases due to the much higher flow rates of plane plumes. Source dimensions involve a slot length of 876 mm, which provides reasonable aspect ratios to maintain a plane flow for the measurements (with maximum values of  $(x-x_0)/b$  in the range 100-200). The source is mounted at the center of a flat floor having a width of 1200 mm, which in turn is attached to side walls having dimensions of 1220 × 2440 mm

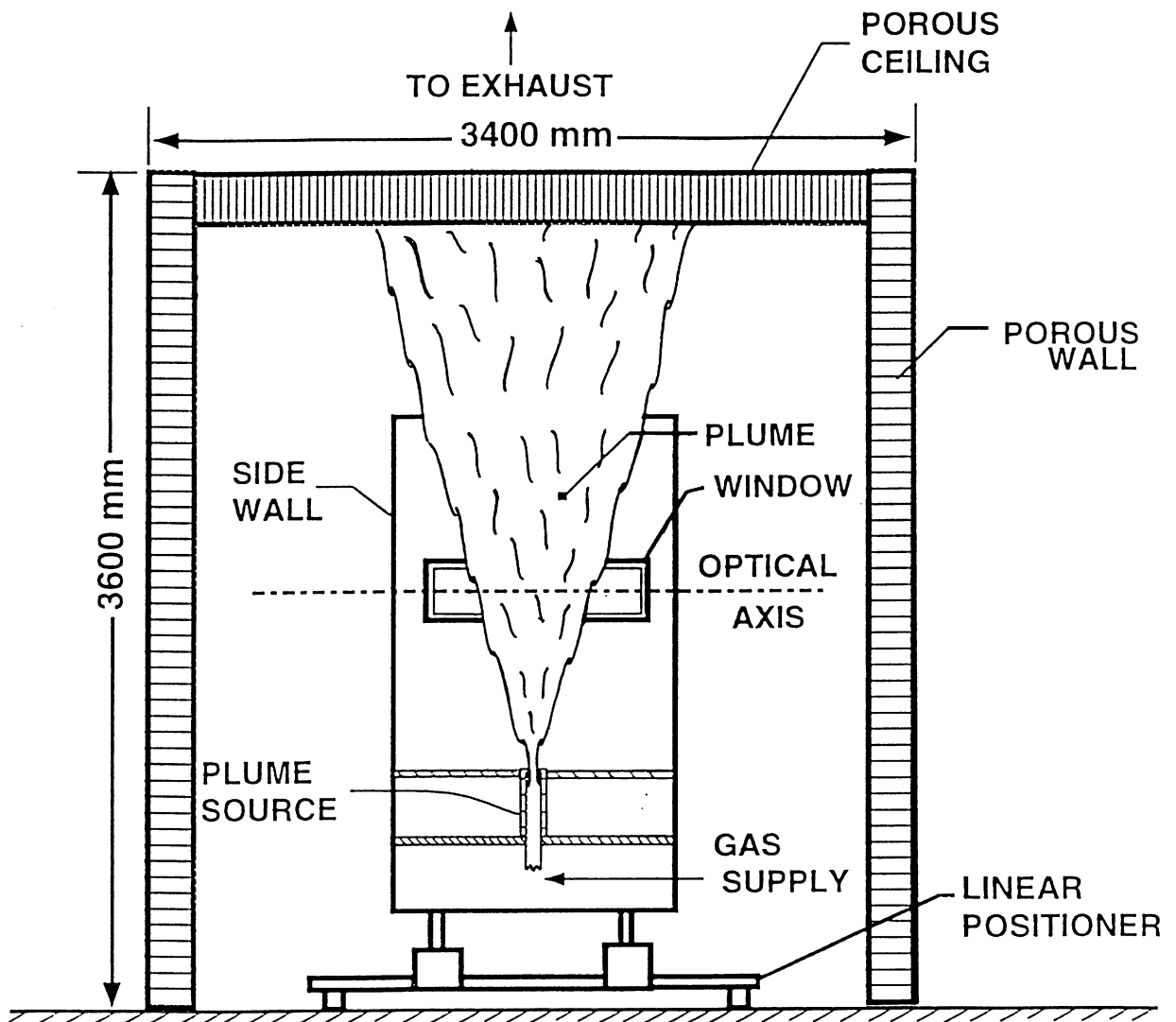


Fig. 18 Sketch of the plane buoyant turbulent plume apparatus.

high. The side walls have fixed windows to provide optical access, with provision made for mounting the source at various heights along the side walls so that values of  $(x-x_0)/b$  can be changed. Horizontal traversing in the cross-stream direction is provided by mounting the entire floor/wall assembly on linear bearings so that it can be moved with a stepping motor-driven linear positioner. Finally, various positions along the slot can be considered, to check for two-dimensionality, by shifting the floor/wall assembly along the linear bearing mount.

The entire apparatus is contained within a windowless room, with the plume itself within a smaller enclosure constructed of either plastic sheets (parallel to the apparatus side walls) or layers of fiberglass filter material (the porous walls shown in Fig. 18 that are parallel to the source slot). In particular, the filter material in the side walls provides for entrained air inflow while avoiding coflow problems within the plume enclosure. The filter material in the ceiling (porous ceiling) provides for outflow of plume gases while preventing leakage of light into the test area from the upper portion of the laboratory. Plume gases are captured in an upper hood, near the ceiling of the laboratory, and are subsequently removed by a blower. The upper hood is separated from the ceiling area of the plume enclosure so that there is no feedback between blower flow rates and plume properties in the test enclosure.

Even with the porous side walls of the apparatus, room disturbances within the experimental enclosure still were a problem; this difficulty manifested itself as an unusually large mixture fraction fluctuation levels near the flow axis. This problem was resolved by installing a pair of 16 mesh screens, separated by a distance of 25 mm, between the outer extremities of the side walls. This approach to control room disturbances for plane free flows (jets) has been used successfully by Gutmark and Wagnanski (1976). The same approach also was used during past work in this laboratory for round self-preserving turbulent plumes (Dai and Faeth, 1996; Dai et al., 1994, 1995a,b). Other modifications of the inner enclosure were studied, i.e., extended side walls, rounded contraction to obtain a smooth flow of entrained fluid at the outer edge of the side walls, and various screen and honeycomb arrangements at the extremities of the side walls. These changes did not have an appreciable effect on the flow, however, and were eliminated in favor of the simplest effective approach for controlling room disturbances as discussed earlier.

The porous ceiling also was somewhat problematical because excessive filter material thickness restricted the flow. This yields an overly thick ceiling layer for the present relatively large source flows so that the ceiling layer interfered with plume flow properties. Modification of the exhaust hood enclosure and the cross-sectional area and thickness of the porous ceiling, however, were able to resolve this difficulty.

The plume gas supply system involved mixing the air and helium flows, which are controlled using critical flow orifices. The source flow then passes through beds of iodine flakes so that it is seeded with iodine for LIF measurements. The source flow then passes through four parallel lines having length-to-diameter ratios greater than 1000 to insure uniform mixing. These flows enter the source manifold and then pass through a bed of glass beads and a contraction to obtain a uniform flow at the slot exit. The final slot passage has variable width capabilities in the range 3-10 mm, using rounded plastic slot closures. All components in contact with the flow after seeding are either plastic or painted to avoid corrosion by iodine. The final exhaust flow leaving through the blower is an

exception, however, because iodine concentrations at this point are less than 100 ppb and cause no corrosion problems.

**Instrumentation.** Measurements thus far have been limited to mean and fluctuating mixture fractions using laser-induced fluorescence (LIF). The main features of these measurements are identical to past work; therefore, Dai et al. (1994,1995a,b) should be consulted for specific details. The approach involves a focused argon-ion laser beam at 514.5 nm (maximum optical power of 1800 mW) while seeding the source flow with iodine vapor. The 514.5 nm line is absorbed naturally by iodine and causes it to fluoresce at longer wavelengths. The fluorescence signal is separated from light scattered from the laser line using long-pass optical filters (cut-off wavelength of 520 nm). The fluorescence signals are observed at right angles to the laser beam using f4.1 collecting optics. The detector outputs are amplified and then low-pass filtered to control alias signals. The signals are then sampled using an a/d converter and transferred to a computer for processing and storage. The detector signals are monitored using a digital oscilloscope, as well.

The LIF signals are calibrated using the flow at the source exit, and mixing this source flow with air to vary the mixture fraction. The LIF signal is not saturated for present conditions and varies directly with laser optical power; therefore, the laser optical power is monitored so that this effect can be considered during data reduction. For present conditions, the laser signal level also varies linearly with mixture fraction for all source flows used thus far.

Differential diffusion among the source gases (helium, iodine and air) can be a significant source of error for LIF measurements. Fortunately, present interest in the self-preserving region of the flow implies relatively large flow Reynolds numbers and negligible effects of differential diffusion compared to experimental uncertainties of roughly 5 and 10% for mean and fluctuating mixture fractions, respectively.

**Test Conditions.** Preliminary tests involved a wide variety of helium-air mixtures, slot widths, initial flow velocities and initial Reynolds numbers in order to develop flows that would rapidly evolve to self-preserving conditions. Not surprisingly, source properties mainly improved as the source Reynolds number was increased. Thus, results reported here involve two sources having the largest possible Reynolds numbers consistent with reasonable costs for helium gas flow to the source.

The operating conditions of the two sources used during the experiments are summarized in Table 8. An attempt has been made to keep source Froude numbers at reasonable levels in order to minimize flow development lengths. The source Reynolds numbers are relatively small 770 and 800 compared to values of 2000 and 4600 for the round plumes but this still yielded reasonable flow development lengths at acceptable gas costs. Present measurements of self-preserving flow properties involved  $(x-x_0)/b \geq 75$  and  $(x-x_0)/\ell_M \geq 6$ ; for these conditions virtual origins proved to be too small to measure accurately and have been assigned values of zero.

### 3.3 Results and Discussion

The present measurements were undertaken as part of apparatus development and involved a variety of source properties, streamwise and lateral positions in the plumes,

Table 8 Plane buoyant turbulent plume test conditions<sup>a</sup>

Source Properties	Source I	Source II
Helium concentration (% by volume)	29	58
Density (kg/m <sup>3</sup> )	0.871	0.581
Kinematic viscosity (mm <sup>2</sup> /s)	22.1	35.0
Slot width (mm)	9.4	9.4
Average velocity (mm/s)	495	732
Reynolds number, $Re_o$	770	800
Froude number, $Fr_o$	3.65	3.40
Morton length scale, $\ell_M / b$	8.0	6.4
Virtual origin based on $\bar{f}$ , $x_o/b$	0.0	0.0

<sup>a</sup>Flow directed vertically upward in still air with ambient pressures and temperature of  $99 \pm 0.5$  kPa and  $297 \pm 0.5$  K. Pure gas properties taken as follows: air density =  $1.161$  kg/m<sup>3</sup>, air kinematic viscosity =  $15.9$  mm<sup>2</sup>/s, helium density = kg/m<sup>3</sup> and helium kinematic viscosity =  $122.5$  mm<sup>2</sup>/s, slot length is 876 mm.

calming screen properties and enclosure properties, as mentioned earlier. All these experiments established satisfactory operating conditions for the results discussed in the following. The present results should be considered to be preliminary pending final measurements and establishment of experimental uncertainties; nevertheless, the present results are not anticipated to be very different from final results.

Plots of the distributions of mean mixture fractions in the cross-stream direction are illustrated in Fig. 19. These results are plotted according to the scaled self-preserving variables for free plane line plumes given in Table 7, considering distances from the source in the range 75-208 source widths, 6-26 Morton length scales, source Reynolds numbers of 770 and 800, and different lateral positions along the source slot to check two-dimensionality (although all these test condition variables are not indicated in the legend of Fig. 19 in order to simplify both the plot and its discussion). Finally, earlier results measured by Rouse et al. (1952), Kotsovinos and List (1977) and Ramaprian and Chandresekhara (1985,1989), all of which are stated to represent self-preserving behavior, are shown on the plot for comparison with the present measurements. For the entire range of conditions illustrated in Fig. 19 it is evident that present measurements yield a narrower flow, with scaled values near the plane of symmetry somewhat smaller, than the earlier results of Rouse et al. (1952), Kotsovinos and List (1977), and Ramaprian and Chandresekhara (1985,1989). It is felt that this disagreement results because self-preserving behavior for plane plumes is only observed at distances somewhat farther from the source than previously thought. Measurements near the source are mainly characterized by a wider distribution of mean mixture fractions in terms of  $y/(x-x_0)$ . In contrast to results for round plumes illustrated in Fig. 14, however, mean mixture fractions near the axis tended to increase nearer to the source, yielding profiles somewhat like those of Rouse et al. (1952), Kotsovinos and List (1977), and Ramparian and Chandresekhara (1985,1989). This suggests that all these sources cause relatively slow development because source Reynolds numbers are small due to problems of providing source conditions for line plumes. This behavior also implies accelerating flow velocities with increasing distances from the source but velocity measurements will be required to establish this behavior.

The tendency for plane turbulent plumes to become narrower in terms of self-preserving variables as they develop, as well as more evidence concerning the state of development of past measurements, can be seen from the mixture fraction fluctuation measurements illustrated in Fig. 20. The range of the present data is the same as mean mixture fraction data shown in Fig. 19. Corresponding measurements of Ramaprian and Chandrasekhara (1989) are also shown on the plot, for the farthest position from their source where they report such data, for comparison with the present measurements. It is clear that self-preserving behavior for the present flow involves significantly narrower flows in terms of turbulence properties than that of Ramaprian and Chandrasekhara (1989) which also exhibit a dip near the plane of symmetry, which is characteristic of the near-source behavior of mixture fraction fluctuations in plumes, see the mixture fraction fluctuation data plotted for round turbulent plumes in Fig. 15. In contrast, present measurements exhibit no such dip near the plane of symmetry and have behavior very similar to round self-preserving plumes. The main difference between the mixture fraction fluctuation distributions of the self-preserving round and plane plumes is that the latter have a slightly larger r.m.s. fluctuation intensity near the axis, i.e. 48% compared to 45%.

Thus, similar to the past work of Dai et al. (1994,1995a,b) for round turbulent plumes, present values of  $(x-x_0)/b$  required to reach self-preserving conditions within plane

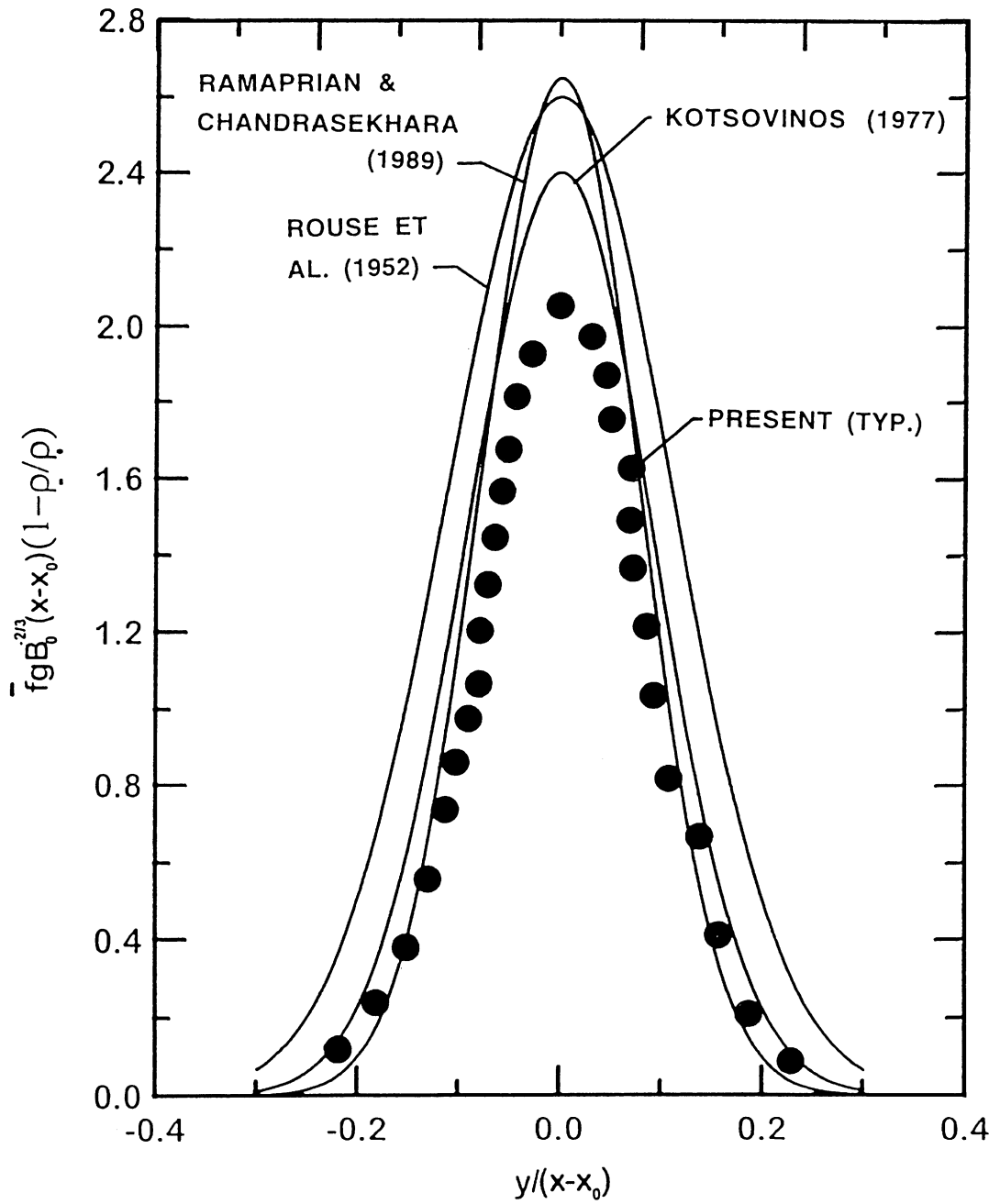


Fig. 19 Cross-stream profiles of mean mixture fractions in plane buoyant turbulent plumes.

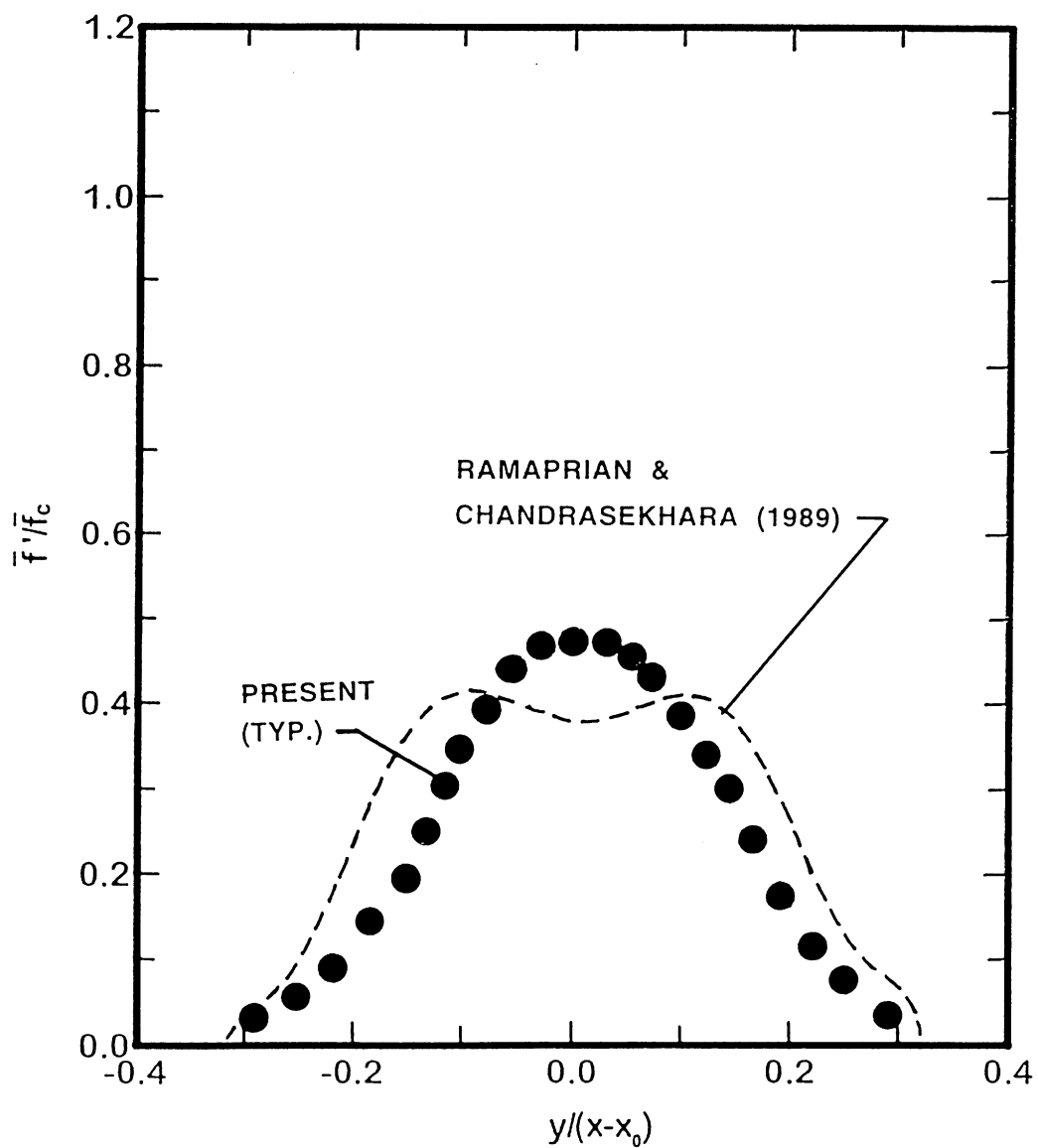


Fig. 20 Cross-stream profiles of r.m.s. fluctuating mixture fractions in plane buoyant turbulent plumes .

turbulent plumes are substantially larger than streamwise distances reached during past measurements of the self-preserving properties of plane turbulent plumes. This behavior is quantified in Table 9. Parameters in the table include the medium,  $(x-x_0)/b$ ,  $(x-x_0)/\ell_M$ ,  $k_f'$ ,  $\ell_f/(x-x_0)$ ,  $F(0)$  and  $(f'/f)_c$ . The parameters  $k_f$  and  $\ell_f$  are characteristics of the flow width based on the assumption that the mean mixture fraction distribution can be approximated by a Gaussian function, as first proposed by Rouse et al. (1952). This yields the following definitions of the flow width parameters;

$$F(y/(x-x_0)) = F(0) \exp \left\{ -k_f^2 (y/(x-x_0))^2 \right\} \quad (11)$$

where

$$k_f = (x-x_0)/\ell_f \quad (12)$$

Thus,  $\ell_f$  represents the characteristic plume half width where  $\bar{f}/\bar{f}_c = \bar{u}/\bar{u}_c = e^{-1}$ .

Somewhat similar to measurements for round turbulent plumes, the widths of the plane turbulent plumes for self-preserving conditions tend to progressively decrease with the date of the study. This yields a conduction of the characteristic plume half width of roughly 50%; in contrast, the scaled mean mixture fraction at the axis tends to decrease by roughly 20% for the plane turbulent plumes rather than increasing as was the case for the round turbulent plumes, see Dai et al. (1994). Flow widths observed by of Ramaprian and Chandrasekhara (1989) are similar to present findings while their scaled mean mixture fraction at the axis is somewhat larger than the present result. This can be explained by reduced levels of turbulence development for the conditions of Ramaprian and Chandrasekhara (1989) as evidenced by reduced mixture fraction fluctuation intensities at the axis compared to present results, i.e. 38% compared to 48%, as discussed earlier.

It is also of interest to compare present results with earlier findings for plane turbulent plumes along surfaces. The wall flow that is most closely related to the present turbulent line plume is the adiabatic wall plume studied by Grella and Faeth (1975). Similar to Rouse et al. (1952), an array of diffusion flames was used to create the line source for the wall plume study so that source widths cannot be defined. In addition, these measurements are never precisely self-preserving because the wall boundary layer scales differently from the outer edge of the plume, although the plume grows much more rapidly than the wall boundary layer and dominates the flow so that approximate self-preserving behavior can still be achieved (Grella and Faeth, 1975). Nevertheless, the measurements of Grella and Faeth (1975) still exhibit systematic variations with height above the source so that the agreement of their results with true self-preserving behavior is somewhat questionable. In spite of these limitations, results for the wall plumes clearly show that the presence of the wall vastly reduces the rate of mixing of the flows. For example, the measurements of Grella and Faeth (1975) for turbulent adiabatic wall plumes yields  $\ell_f/(x-x_0) = 0.07$  and  $F(0) = 5.70$  compared with present results for free turbulent plane plumes in Table 9 which yields  $\ell_f/(x-x_0) = 0.11$  and  $F(0) = 2.06$ . Failure to completely reach self-preserving conditions for the adiabatic wall plumes is unlikely to explain a difference of this magnitude; instead, inhibition of large-scale motion by the presence of the wall appears to be a more likely reason for this effect. Additional study of these differences is clearly merited, however, in order to gain a better understanding of effects of the motion of large turbulent eddies on turbulent mixing rates in buoyant turbulent flows.

Table 9 Summary of self-preserving plane turbulent plume constants<sup>a</sup>

Source	Present Study	Ramapiran and Chandrasekhara (1989)	Kotsovinos (1977)	Rouse et al. (1952) <sup>b</sup>
Medium	gas	liquid	liquid	gas
$(x-x_0)/b$	75-208	20-60	6-30	---
$(x-x_0)/\ell_M$	10-26	3-15	2.3-122	---
$k_f^2$	83	83	59	41
$\ell_f/(x-x_0)$	0.11	0.11	0.14	0.16
F(0)	20.06	2.65	2.40	2.60
$(\bar{f}'/\bar{f})_c$	0.48	0.42	---	---

<sup>a</sup>Plane turbulent plumes in still and unstratified environments. Range of streamwise distances are for conditions where quoted self-preserving properties were found from measurements over the cross-section of the flames. Entries are ordered chronologically.  
<sup>b</sup>Source involved a linear array of combusting round jets so that slot width cannot be defined.

### 3.4 Conclusions

The structure and mixing properties of plane turbulent plumes were studied experimentally, emphasizing behavior for self-preserving conditions where effects of source disturbances are lost and flow properties scale in a relatively simple manner. Test conditions involved buoyant jet sources of helium/air mixtures with  $(x-x_0)/b$  in the range 75-208 and  $(x-x_0)/\ell_M$  in the range 6-26. The major conclusions of the study are as follows:

1. The present measurements yielded distributions of mean mixture fractions in self-preserving plumes that were up to 50% narrower, with scaled values at the plane of symmetry that differed by as much as 20%, from other results using buoyant jet sources in the literature, e.g., Ramaprian and Chandrasekhara (1989), Kotsovinos (1977) and Rouse et al. (1952). Based on present observations, it appears that the earlier results were still in the transitional regime and were not obtained at sufficient distances from the source to reach self-preserving conditions.
2. Cross-stream distributions of mixture fraction fluctuations in the self-preserving region of plane turbulent plumes does not exhibit reduced values near the plane of symmetry similar to plane jets. Instead, effects of buoyancy cause mixture fraction fluctuations to reach a maximum at the plane of symmetry, with intensities of roughly 48%. These values are comparable to results observed in self-preserving round turbulent plumes, 45%, and are strong evidence of significant effects of buoyancy/turbulence interactions in these flows.
3. Characteristic flow widths are smaller, and scaled mean mixture properties,  $F(0)$ , are larger for adiabatic turbulent wall plumes than for the present free plane turbulent plumes: e.g.,  $\ell_f/(x-x_0) = 0.07$  and  $0.11$  while  $F(0) = 5.70$  and  $2.06$  for wall and free plumes, respectively. While it should be noted that there is some question about whether existing adiabatic turbulent wall plume measurements properly achieved self-preserving behavior, it is still very likely that these large reductions of turbulent mixing rates for the wall plumes are due to effects of the wall inhibiting large-scale turbulent motion.

It should be emphasized that present results represent preliminary estimates found during an extensive series of experiments to establish effects of source and enclosure properties or flow properties. Current work is establishing final results, as well as considering other flow properties of interest, e.g., probability density functions, spectra, correlations and scales of mixture fraction fluctuations; corresponding properties for flow velocities will be found, as well, if time permits.

### References

- Abraham, G. (1960) "Jet Diffusion in Liquid of Greater Density," ASCE J. Hyd. Dev., Vol. 86, pp. 1-13.
- Batten, C.E. (1985) "Spectral Optical Constants of Soots from Polarized Angular Reflectance Measurements," Appl. Optics, Vol. 24, pp. 1193-1199.
- Becker, H.A., Hottel, H.C., and Williams, G.C. (1967) "The Nozzle-Fluid Concentration Field of the Round, Turbulent, Free Jet." J. Fluid Mech., Vol. 30, pp. 285-303.

Berry, M. V., and Percival, I. C. (1986) "Optics of Fractal Clusters Such as Smoke," Optica Acta, Vol. 33, pp. 577-591.

Chang, H.Y., and Charalampopoulos, T. T. (1990) "Determination of the Wavelength Dependence of Refractive Indices of Flame Soot," Proc. R. Soc. London A, Vol. 430, pp. 577-591.

Charalampopoulos, T.T. (1992) "Morphology and Dynamics of Agglomerated Particulates in Combustion Systems Using Light Scattering Techniques," Prog. Energy Combust. Sci., Vol. 18, pp. 13-45.

Choi, M.Y., Hamins, A., Mulholland, G.W., and Kashiwagi, T. (1994) "Simultaneous Optical Measurement of Soot Volume Fraction and Temperature," Combust. Flame, Vol. 99, pp. 174-186.

Choi, M.Y., Hamins, A., Mulholland, G.W., and Kashiwagi, T. (1995) "Comparisons of the Soot Volume Fraction using Gravimetric and Light Extinction Techniques," Combust. Flame, Vol. 102, pp. 161-169

Dai, Z., and Faeth, G.M. (1996) "Measurements of the Structure of Self-Preserving Round Buoyant Turbulent Plumes," J.Heat Trans., Vol. 118, No. 2, pp. 493-495..

Dai, Z., Tseng, L.-K., and Faeth, G.M. (1994) "Structure of Round, Fully-Developed, Buoyant Turbulent Plumes," J. Heat Trans., Vol. 116, No. 2, pp. 409-417.

Dai, Z., Tseng, L.-K., and Faeth, G.M. (1995a) "Velocity Statistics of Round, Fully-Developed Buoyant Turbulent Plumes," J. Heat Transfer, Vol. 117, No. 1, pp. 138-145.

Dai, Z., Tseng, L.-K., and Faeth, G. M. (1995b) "Velocity/Mixture-Fraction Statistics of Round, Self-Preserving Buoyant Turbulent Plumes," J. Heat Trans., Vol. 117, No. 4, pp. 918-926.

Dalzell, W.H., and Sarofim, A.F. (1969) "Optical Constants of Soot and Their Application to Heat Flux Calculations," J. Heat Trans. Vol. 91, No. 1, pp. 100-104.

Dalzell, W.H., Williams, G.C., and Hottel, H.C. (1970), "A Light Scattering Method for Soot Concentration Measurements," Combust. Flame, Vol. 14, pp. 161-170.

Dobbins, R.A., and Megaridis, C.M. (1987) "Morphology of Flame-Generated Soot as Determined by Thermophoretic Sampling," Langmuir, Vol. 3, pp. 254-259.

Dobbins, R.A., and Megaridis, C.M. (1991) "Absorption and Scattering of Light by Polydisperse Aggregates," Appl. Optics, Vol. 30, pp. 4747-4754.

Dobbins, R.A., Mulholland, G.W., and Bryner, N.P. (1993) "Comparison of a Fractal Smoke Optics Model with Light Extinction Measurements," Atmospheric Environment, Vol. 28, pp. 889-897.

Dyer, T.M. (1979) "Rayleigh Scattering Measurements of Time-Resolved Concentration in a Turbulent Propane Jet," AIAAJ., Vol. 17, pp. 912-914.

Erickson, W.D., Williams, G.C., and Hottel, H.C. (1964) "Light Scattering Measurements on Soot in a Benzene-Air Flame," Combust. Flame, Vol. 8, pp. 127-132.

- Faeth, G.M. (1997) "Optical and Radiative Properties of Soot in Flame Environments," Prog. Energy Combust. Sci., in press.
- Faeth, G.M., and Köylü, Ü.Ö. (1995) "Soot Morphology and Optical Properties in Nonpremixed Turbulent Flame Environments," Combust.Sci. Tech., Vol. 108, pp. 207-229.
- Faeth, G.M., and Köylü, Ü.Ö. (1996) "Structure and Optical Properties of Flame-Generated Soot," *Transport Phenomena in Combustion* (S.H. Chan, ed.), Taylor & Francis, Washington, Vol. 1, pp. 19-44.
- Faeth, G.M., Gore, J.P., Chuech, S.G., and Jeng, S.-M. (1989). "Radiation from Turbulent Diffusion Flames," *Annual Review of Numerical Fluid Mechanics and Heat Transfer*, Vol. 2, Hemisphere Publishing Corp., Washington, pp. 1-38.
- Faeth, G.M., Kounalakis, M.E., and Sivathanu, Y.R. (1990) "Stochastic Aspects of Turbulent Combustion Processes," Chemometrics and Intelligent Laboratory Systems, Vol. 10, pp. 199-210.
- Farias, T., Carvalho, M.G., Köylü, Ü.Ö., and Faeth, G.M. (1995) "Computational Evaluation of Approximate Rayleigh-Debye-Gans/Fractal-Aggregate Theory for the Absorption and Scattering of Light by Aggregated Small Particles." J. Heat Trans., Vol. 117, No. 1, pp. 152-159.
- Felske, J.D., Charalampopoulos, T.T., and Hura, H. (1984) "Determination of the Refractive Indices of Soot Particles from the Reflectivities of Compressed Soot Pellets," Combust. Sci. Tech. Vol. 37, p. 263.
- George, W.K., Jr., Alpert, R.L., and Tamanini, F. (1977) "Turbulence Measurements in an Axisymmetric Buoyant Plume," Int. J. Heat Mass Trans., Vol. 20, pp. 1145-1154.
- Gore, J.P., and Faeth, G.M. (1986) "Structure and Spectral Radiation Properties of Turbulent Ethylene/Air Diffusion Flames," *Twenty-First Symposium (International) on Combustion*, The Combustion Institute, Pittsburgh, pp. 1521-1531.
- Gore, J.P., and Faeth, G.M. (1988) "Structure and Radiation Properties of Luminous Turbulent Acetylene/Air Diffusion Flames," J. Heat Trans., Vol. 110, No. 1, pp. 173-181.
- Grella, J.J., and Faeth, G.M. (1975) "Measurements in a Two-Dimensional Thermal Plume Along a Vertical Adiabatic Wall," J. Fluid Mech., Vol. 71, Part 4, pp. 701-710.
- Gutmark, E., and Wygnanski, I. (1976) "The Plane Turbulent Jet," J. Fluid Mech., Vol. 73, Part 3, pp. 465-495.
- Hinze, J. O. (1975) *Turbulence*, 2nd ed., McGraw-Hill, New York, pp. 175-319.
- Iskander, M.F., Chen, H.Y., and Penner, J.E. (1989) "Optical Scattering and Absorption by Branched Chains of Aerosols," Appl. Optics, Vol. 28, pp. 3083-3091.
- Jullien, R., and Botet, R. (1987) *Aggregation and Fractal Aggregates*, World Scientific Publishing Co., Singapore, pp. 45-60.
- Kotsovinos, N.E. (1977) "Plane Turbulent Buoyant Jets. Part 2. Turbulence Structure," J. Fluid Mech., Vol. 81, pp. 45-62.

Kotsovinos, N.E. (1985) "Temperature Measurements in a Turbulent Round Plume," Int. J. Heat Mass Trans., Vol. 28, pp. 771-777.

Kotsovinos, N.E., and List, E.J. (1977) "Turbulent Buoyant Jets. Part 1. Integral Properties," J. Fluid Mech., Vol. 81, pp. 25-44.

Köylü, Ü.Ö. (1992), "Emission, Structure and Optical Properties of Overfire Soot from Buoyant Turbulent Diffusion Flames," Ph.D. Thesis, The University of Michigan, Ann Arbor, Michigan.

Köylü, Ü.Ö., and Faeth, G.M. (1991) "Carbon Monoxide and Soot Emissions from Liquid-Fueled Buoyant Turbulent Diffusion Flames," Combust. Flame, Vol. 87, No. 1, pp. 61-76.

Köylü, Ü.Ö., and Faeth, G.M. (1992) "Structure of Overfire Soot in Buoyant Turbulent Diffusion Flames at Long Residence Times," Combust. Flame, Vol. 89, No. 2, pp. 140-156.

Köylü, Ü.Ö., and Faeth, G.M. (1993) "Radiative Properties of Flame-Generated Soot," J. Heat Trans., Vol. 115, No. 2, pp. 409-417.

Köylü, Ü.Ö., and Faeth, G.M. (1994a) "Optical Properties of Overfire Soot in Buoyant Turbulent Diffusion Flames at Long Residence Times," J. Heat Trans. Vol. 116, No. 1, pp. 152-159.

Köylü, Ü.Ö., and Faeth, G.M. (1994b) "Optical Properties of Soot in Buoyant Laminar Diffusion Flames," J. Heat Trans., Vol. 116, pp. 971-979.

Köylü, Ü.Ö., and Faeth, G.M. (1996) "Spectral Extinction Coefficients of Soot Aggregates from Turbulent Diffusion Flames," J. Heat Trans., Vol. 118, No. 2, pp. 415-421.

Köylü, Ü.Ö., Sivathanu, Y., and Faeth, G.M. (1991) "Carbon Monoxide Emissions from Buoyant Turbulent Diffusion Flames," *Third International Symposium on Fire Safety Science*, Elsevier, London, pp. 625-634.

Köylü, Ü.Ö., Faeth, G.M., Farias, T.L., and Carvalho, M.G. (1996) "Fractal and Projected Structure Properties of Soot Aggregates," Combust. Flame, Vol. 100, No. 4, pp. 621-633.

Krishnan, S.S., Lin, K.-C., Wu, J.-S., and Faeth, G.M. (1997) "Optical Properties in the Visible of Soot Emitted from Turbulent Pool Fires," 1997 ASME Winter Annual Meeting, submitted.

Ku, J.C., and Felski, J.D. (1986) "Determination of Refractive Indices of Mie Scatterers from Kramers-Kronig Analysis of Spectral Extinction Dat," J. Opt. Soc. Am., Vol. 3, pp. 617-623.

Ku, J.C., and Shim, K.-H. (1992) "A Comparison of Solutions for Light Scattering and Absorption by Agglomerated or Arbitrarily-Shaped Particles," J. Quant. Spect. and Rad. Trans., Vol. 47, pp. 201-220.

- Lai, M.-C., and Faeth, G.M. (1987a) "Turbulence Structure of Vertical Adiabatic Wall Plumes," J. Heat Trans., Vol. 109, pp. 663-670.
- Lai, M.-C., and Faeth, G.M. (1987b) "A Combined Laser-Doppler Anemometer/Laser-Induced Fluorescence System for Turbulent Transport Measurements," J. Heat Trans. Vol. 109, pp. 254-256.
- Lai, M.-C., Jeng, S.-M., and Faeth, G.M. (1986) "Structure of Turbulent Adiabatic Wall Plumes," J. Heat Trans., Vol. 108, pp. 827-834.
- Lee, S.C., and Tien, C.L. (1980) "Optical Constants of Soot in Hydrocarbon Flames," *Eighteenth Symposium (International) on Combustion*, The Combustion Institute, Pittsburgh, pp. 1159-1166.
- Lee, S.C., and Tien, C.L. (1983) "Effect of Soot Shape on Soot Radiation," J. Quant. Spectrosc. Radiat. Transfer, Vol. 29, pp. 259-265.
- Liburdy, J.A., and Faeth, G.M. (1978) "Heat Transfer and Mean Structure of a Turbulent Thermal Plume Along Vertical Isothermal Walls," J. Heat Trans., Vol. 100, pp. 177-183.
- Liburdy, J.A., Groff, E.G., and Faeth, G.M. (1979) "Structure of a Turbulent Thermal Plume Rising Along an Isothermal Wall," J. Heat Trans., Vol. 101, pp. 299-255.
- List, E.J. (1982) "Turbulent Jets and Plumes," Ann. Rev. Fluid Mech., Vol. 14, pp. 189-212.
- Lou, W., and Charalampopoulos, T.T. (1994) "On the Electromagnetic Scattering and Absorption of Agglomerated Small Spherical Particles," J. Phys. D: Appl. Phys., Vol. 27, pp. 2258-2270.
- Martin, J.E., and Hurd, A.J. (1987) "Scattering from Fractals," J. Appl. Cryst., Vol. 20, pp. 61-78.
- Medalia, A.I., and Heckman, F.A. (1969) "Morphology of Aggregates — II. Size and Shape Factors of Carbon Black Aggregates from Electron Microscopy," Carbon, Vol. 7, pp. 567-582.
- Megaridis, C.M., and Dobbins, R.A. (1989) "Comparison of Soot Growth and Oxidation in Smoking and Nonsmoking Ethylene Diffusion Flames," Combust. Sci. Tech., Vol. 66, No. 1, pp. 1-16.
- Megaridis, C.M., and Dobbins, R.A. (1990) "Morphological Description of Flame-Generated Materials," Combust. Sci. Tech., Vol. 71, pp. 95-109.
- Mizushima, T., Ogino, F., Veda, H., and Komori, S. (1979) "Application of Laser-Doppler Velocimetry to Turbulence Measurements in Non-Isothermal Flow," Proc. Roy. Soc. London, Vol. A366, pp. 63-79.
- Morton, B.R. (1959) "Forced Plumes," J. Fluid Mech., Vol. 5, pp. 151-163.
- Morton, B.R., Taylor, G.I., and Turner, J.S. (1956) "Turbulent Gravitational Convection from Maintained and Instantaneous Sources," Proc. Roy. Soc. London, Vol. A234, pp. 1-23.

- Mountain, R.D., and Mulholland, G.W. (1988) "Light Scattering from Simulated Smoke Agglomerates," Langmuir, Vol. 4, pp. 1321-1326.
- Mulholland, G.W., Samson, R.J., Mountain, R.D., and Ernst, M.H. (1988) "Cluster Size Distribution for Free Molecular Aggregation," J. Energy Fuels, Vol. 2, pp. 481-486.
- Nakagome, H., and Hirata, M. (1977) "The Structure of Turbulent Diffusion in an Axisymmetrical Thermal Plume," *Heat Transfer and Turbulent Buoyant Convection* (D.B. Spalding and N. Afgan, eds.), McGraw-Hill, New York, pp. 367-372.
- Nelson, J. (1989a) "Test of a Mean Field Theory for the Optics of Fractal Clusters," J. Modern Optics, Vol. 36, pp. 1031-1057.
- Nelson, J. (1989b) "Fractality of Sooty Smoke: Implications for the Severity of Nuclear Winter," Nature, Vol. 339, pp. 611-613.
- Ogino, F., Takeuchi, H., Kudo, I., and Mizushima, T. (1980) "Heated Jet Discharged Vertically in Ambients of Uniform and Linear Temperature Profiles," Int. J. Heat Mass Trans., Vol. 23, pp. 1581-1588.
- Panchapakesan, N.R., and Lumley, J.L. (1993) "Turbulence Measurements in Axisymmetric Jets of Air and Helium. Part 2. Helium Jet," J. Fluid Mech., Vol. 246, pp. 225-247.
- Papanicolaou, P.N., and List, E.J. (1987) "Statistical and Spectral Properties of Tracer Concentration in Round Buoyant Jets," Int. J. Heat Mass Trans., Vol. 30, pp. 2059-2071.
- Papanicolaou, P.N., and List, E.J. (1988) "Investigation of Round Vertical Turbulent Buoyant Jets," J. Fluid Mech., Vol. 195, pp. 341-391.
- Papantoniou, D., and List, E.J. (1989) "Large Scale Structure in the Far Field of Buoyant Jets," J. Fluid Mech., Vol. 209, pp. 151-190.
- Peterson, J., and Bayazitoglu, Y. (1992) "Measurements of Velocity and Turbulence in Vertical Axisymmetric Isothermal and Buoyant Plumes," J. Heat Trans., Vol. 114, pp. 135-142.
- Pitts, W.M., and Kashiwagi, T. (1984) "The Application of Laser-Induced Rayleigh Light Scattering to the Study of Turbulent Mixing," J. Fluid Mech., Vol. 141, pp. 391-429.
- Pivovarov, M.A., Zhang, H., Ramaker, D.E., Tatem, P.A., and Williams, F.W. (1992) "Similarity Solutions in Buoyancy-Controlled Diffusion Flame Modelling," Combust. Flame, Vol. 92, pp. 308-319.
- Ramaprian, B.R., and Chandrasekhara, M.S. (1985) "LDA Measurements in Plane Turbulent Jets," J. Fluids Engr., Vol. 107, pp. 264-271.
- Ramaprian, B.R., and Chandrasekhara, M.S. (1989) "Measurements in Vertical Plane Turbulent Plumes," J. Fluids Engr., Vol. 111, pp. 69-77.
- Rosner, D.E., Mackowski, D.W., and Garcia-Ybarra, P. (1991) "Size- and Structure-Insensitivity of the Thermophoretic Transport of Aggregated 'Soot' Particles in Gases," Combust. Sci. Tech., Vol. 80, No. 1, pp. 87-101.

- Rouse, H., Yih, C.S., and Humphreys, H.W. (1952) "Gravitational Convection from a Boundary Source," Tellus, Vol. 4, pp. 201-210.
- Rudder, R.R., and Bach, D. R. (1968) "Rayleigh Scattering of Ruby-Laser Light by Neutral Gases," J. Opt. Soc. Amer., Vol. 58, pp. 1260-1266.
- Samson, R. J., Mulholland, G. W., and Gentry, J. W. (1987) "Structural Analysis of Soot Agglomerates," Langmuir, Vol. 3, pp. 272-281.
- Seban, R.A., and Behnia, M.M. (1976) "Turbulent Buoyant Jets in Unstratified Surroundings," Int. J. Heat Mass Trans., Vol. 19, pp. 1197-1204.
- Shabbir, A. (1987) "An Experimental Study of an Axisymmetric Turbulent Buoyant Plume and Evaluation of Closure Hypotheses," Ph.D. Thesis, SUNY-Buffalo.
- Shabbir, A., and George, W.K. (1992) "Experiments on a Round Turbulent Buoyant Plume," NASA Technical Memorandum 105955.
- Shabbir, A., and Taulbee, D.B. (1990) "Evaluation of Turbulence Models for Predicting Buoyant Flows," J. Heat Trans., Vol. 112, pp. 945-951.
- Sivathanu, Y.R., and Faeth, G.M. (1990) "Soot Volume Fractions in the Overfire Region of Turbulent Diffusion Flames," Combust. Flame, Vol. 81, No. 2, pp. 133-149.
- Sorensen, C.M., Cai, J., and Lu, N. (1992a) "Test of Static Structure Factors for Describing Light Scattering from Fractal Soot Aggregates," Langmuir, Vol. 8, pp. 2064-2069.
- Sorensen, C.M., Cai, J., and Lu, N. (1992b) "Light-Scattering Measurements of Monomer Size, Monomers per Aggregate, and Fractal Dimension for Soot Aggregates in Flames," Applied Optics, Vol. 31, pp. 6547-6557.
- Stagg, B.J., and Charalampopoulos, T.T. (1990) "Method to Minimize the Effects of Polarizer Leakage on Reflectivity Measurements," Appl. Optics, Vol. 29, pp. 4638-4645.
- Stagg, B.J., and Charalampopoulos, T.T. (1991) "Surface-Roughness Effects on the Determination of Optical Properties of Materials by the Reflection Method," Appl. Optics, Vol. 30, pp. 113-4118.
- Stagg, B.J., and Charalampopoulos, T.T. (1993) "Refractive Indices of Pyrolytic Graphite, Amorphous Carbon, and Flame Soot in the Temperature Range 25° to 600° C.," Combust. Flame, Vol. 94, pp. 381-396.
- Sugiyama, G. (1994) "Nonluminous Diffusion Flame of Diluted Acetylene in Oxygen Enriched Air," *Twenty-fifth Symposium (International) on Combustion*, The Combustion Institute, Pittsburgh, pp. 601-608.
- Tennekes, H., and Lumley, J.L. (1972) *A First Course in Turbulence*, MIT Press, Cambridge, Massachusetts, pp. 113-124.
- Tien, C. L., and Lee, S. C. (1982) "Flame Radiation," Prog. Energy Combust. Sci., Vol. 8, pp. 41-59.

Vaglieco, B.M., Beretta, F., and D'Alessio, A. (1990) "In Situ Evaluation of the Soot Refractive Index in the uv-Visible from the Measurements of Scattering and Extinction Coefficients in Rich Flames," Combust. Flame, Vol. 9, pp. 259-271.

Viskanta, R., and Mengüç, M.P. (1987) "Radiation Heat Transfer in Combustion Systems," Prog. Energy Combust. Sci., Vol. 13, pp. 97-160.

Wersborg, B.L., Howard, J.B., and Williams, G.C. (1972) "Physical Mechanisms in Carbon Formation in Flames," *Fourteenth Symposium (International) on Combustion*, The Combustion Institute, Pittsburgh, pp. 929-940.

Wu, J.-S., Krishnan, S.S., and Faeth, G.M. (1997) "Refractive Indices at Visible Wavelengths of Soot Emitted from Buoyant Turbulent Diffusion Flames," J. Heat Trans., in press.

Zimin, V.D., and Frik, P.G. (1977) "Averaged Temperature Fields in Asymmetrical Turbulent Streams over Localized Heat Sources," Izv. Akad. Nauk. SSSR, Mekhanika Zhidkosti Gaza, Vol. 2, pp. 199-203.

NIST-114 (REV. 11-94) ADMAN 4.09	U.S. DEPARTMENT OF COMMERCE NATIONAL INSTITUTE OF STANDARDS AND TECHNOLOGY	(ERB USE ONLY)	
<b>MANUSCRIPT REVIEW AND APPROVAL</b>		ERB CONTROL NUMBER  	DIVISION  
INSTRUCTIONS: ATTACH ORIGINAL OF THIS FORM TO ONE (1) COPY OF MANUSCRIPT AND SEND TO THE SECRETARY, APPROPRIATE EDITORIAL REVIEW BOARD.		PUBLICATION REPORT NUMBER <b>NIST-GCR-97-721</b>	CATEGORY CODE  
TITLE AND SUBTITLE (CITE IN FULL) <b>Mixing and Radiation Properties of Buoyant Luminous Flame Environments</b>		PUBLICATION DATE <b>July, 1997</b>	NUMBER PRINTED PAGES  
CONTRACT OR GRANT NUMBER  <b>60NANB4D1696</b>	TYPE OF REPORT AND/OR PERIOD COVERED  <b>October, 1996</b>		
AUTHOR(S) (LAST NAME, FIRST INITIAL, SECOND INITIAL)  <b>Dai, Z.; Krishnan, S.S.; Lin, K.-C.; Sangras, R.; Wu, J.S.; Faeth, G.M</b>	PERFORMING ORGANIZATION (CHECK (X) ONE BLOCK) <input checked="" type="checkbox"/> NIST/GAITHERSBURG <input type="checkbox"/> NIST/BOULDER <input type="checkbox"/> JILA/BOULDER		
LABORATORY AND DIVISION NAMES (FIRST NIST AUTHOR ONLY)  SPONSORING ORGANIZATION NAME AND COMPLETE ADDRESS (STREET, CITY, STATE, ZIP) <b>Department of Commerce          National Institute of Standards and Technology          Gaithersburg, MD</b>			
PROPOSED FOR NIST PUBLICATION <input type="checkbox"/> JOURNAL OF RESEARCH (NIST JRES) <input type="checkbox"/> MONOGRAPH (NIST MN) <input type="checkbox"/> LETTER CIRCULAR <input type="checkbox"/> J. PHYS. & CHEM. REF. DATA (JPCRD) <input type="checkbox"/> NATL. STD. REF. DATA SERIES (NIST NSRDS) <input type="checkbox"/> BUILDING SCIENCE SERIES <input type="checkbox"/> HANDBOOK (NIST HB) <input type="checkbox"/> FEDERAL INF. PROCESS. STDS. (NIST FIPS) <input type="checkbox"/> PRODUCT STANDARDS <input type="checkbox"/> SPECIAL PUBLICATION (NIST SP) <input type="checkbox"/> LIST OF PUBLICATIONS (NIST LP) <input checked="" type="checkbox"/> OTHER <b>NIST-GCR</b> <input type="checkbox"/> TECHNICAL NOTE (NIST TN) <input type="checkbox"/> NIST INTERAGENCY/INTERNAL REPORT (NISTIR)			
PROPOSED FOR NON-NIST PUBLICATION (CITE FULLY) <input type="checkbox"/> U.S. <input type="checkbox"/> FOREIGN		PUBLISHING MEDIUM <input type="checkbox"/> PAPER <input type="checkbox"/> CD-ROM <input type="checkbox"/> DISKETTE (SPECIFY) _____ <input type="checkbox"/> OTHER (SPECIFY) _____	
SUPPLEMENTARY NOTES  			
ABSTRACT (A 2000-CHARACTER OR LESS FACTUAL SUMMARY OF MOST SIGNIFICANT INFORMATION. IF DOCUMENT INCLUDES A SIGNIFICANT BIBLIOGRAPHY OR LITERATURE SURVEY, CITE IT HERE. SPELL OUT ACRONYMS ON FIRST REFERENCE.) (CONTINUE ON SEPARATE PAGE, IF NECESSARY.)  <b>An investigation of the radiation and mixing properties of buoyant turbulent diffusion flames is described. The study was divided into two phases: (1) the consideration of the optical and radiative properties of soot, which must be understood in order to develop nonintrusive methods for measuring soot properties and to estimate the continuum radiation properties of soot in flame environments, and (2) the consideration of the structure and mixing properties of buoyant turbulent plumes, which must be understood in order to resolve effects of turbulent/radiation interactions and benchmark computationally tractable models of buoyant turbulent flows.</b>			
KEY WORDS (MAXIMUM OF 9; 28 CHARACTERS AND SPACES EACH; SEPARATE WITH SEMICOLONS; ALPHABETIC ORDER; CAPITALIZE ONLY PROPER NAMES) <b>buoyant plumes, diffusion flames, fire research optical properties, soot, soot aggregates, turbulent flames, turbulent mixing</b>			
AVAILABILITY <input type="checkbox"/> UNLIMITED <input type="checkbox"/> FOR OFFICIAL DISTRIBUTION - DO NOT RELEASE TO NTIS <input type="checkbox"/> ORDER FROM SUPERINTENDENT OF DOCUMENTS, U.S. GPO, WASHINGTON, DC 20402 <input type="checkbox"/> ORDER FROM NTIS, SPRINGFIELD, VA 22161		NOTE TO AUTHOR(S): IF YOU DO NOT WISH THIS MANUSCRIPT ANNOUNCED BEFORE PUBLICATION, PLEASE CHECK HERE. <input type="checkbox"/>	